Circulation Research
JOURNAL OF THE AMERICAN HEART ASSOCIATION

American Heart Association®
Learn and Live℠

Examining Intracellular Organelle Function Using Fluorescent Probes: From Animalcules to Quantum Dots

Dmitry B. Zorov, Evgeny Kobrinsky, Magdalena Juhaszova and Steven J. Sollott

Circ. Res. 2004;95;239-252
DOI: 10.1161/01.RES.0000137875.42385.8e
Circulation Research is published by the American Heart Association. 7272 Greenville Avenue, Dallas, TX 72514
Copyright © 2004 American Heart Association. All rights reserved. Print ISSN: 0009-7330. Online ISSN: 1524-4571

The online version of this article, along with updated information and services, is located on the World Wide Web at:
http://circres.ahajournals.org/cgi/content/full/95/3/239

Data Supplement (unedited) at:
http://circres.ahajournals.org/cgi/content/full/95/3/239/DC1

Subscriptions: Information about subscribing to Circulation Research is online at
http://circres.ahajournals.org/subscriptions/

Permissions: Permissions & Rights Desk, Lippincott Williams & Wilkins, a division of Wolters Kluwer Health, 351 West Camden Street, Baltimore, MD 21202-2436. Phone: 410-528-4050. Fax: 410-528-8550. E-mail:
journalpermissions@lww.com

Reprints: Information about reprints can be found online at
http://www.lww.com/reprints

Downloaded from circres.ahajournals.org by on May 24, 2010

This Review is part of a thematic series on Imaging of Cardiovascular Cells and Tissues, which includes the following articles:

Use of Chimeric Fluorescent Proteins and FRET to Monitor Cellular Responses

Imaging Microdomain Ca^{2+} in Muscle Cells

Optical Imaging of the Heart

Examining Intracellular Organelle Function Using Fluorescent Probes

Two-Photon Microscopy of Cells and Tissues

Brian O'Rourke, Guest Editor

Examining Intracellular Organelle Function Using Fluorescent Probes

From Animalcules to Quantum Dots

Dmitry B. Zorov, Evgeny Kobrinsky, Magdalena Juhaszova, Steven J. Sollott

Abstract—Fluorescence microscopy imaging has become one of the most useful techniques to assess the activity of individual cells, subcellular trafficking of signals to and between organelles, and to appreciate how organelle function is regulated. The past 2 decades have seen a tremendous advance in the rational design and development in the nature and selectivity of probes to serve as reporters of the intracellular environment in live cells. These probes range from small organic fluorescent molecules to fluorescent biomolecules and photoproteins ingeniously engineered to follow signaling traffic, sense ionic and nonionic second messengers, and report various kinase activities. These probes, together with recent advances in imaging technology, have enabled significantly enhanced spatial and temporal resolution. This review summarizes some of these developments and their applications to assess intracellular organelle function. **(*Circ Res*. 2004;95:239-252.)**

Key Words: microscopy ■ calcium ■ redox ■ mitochondria ■ fluorescent proteins

Responses of single cells undergoing physiological activation processes or pathological stresses can be quite heterogeneous in time and space. Measurements of these parameters in bulk (such as in tissue or cellular suspension), using conventional physiological and biochemical methods, can often fail to resolve discrete differences in the kinetics and magnitudes of the responses between cells, as well as complex intracellular and subcellular dynamical processes, critical to understanding how cells actually work. For example, during embryonic development or periods of environmental stress, the decision for a certain cell to undergo apoptosis may be triggered in a moment and distinct from its neighbors, the resulting intracellular processes may proceed along a more or less protracted time frame, and these events may occur heterogeneously among (and inside) other cells. Yet, bulk measures of the progression of apoptosis, such as by DNA-laddering, although undeniably valuable, would show only the overall slow progression with time. All-or-none phenomenon occurring in discrete organelles, such as the mitochondrial permeability transition (MPT), appears as a graded response when examined in bulk suspensions of cells or mitochondria. Similar arguments can be made for resolving questions of Ca^{2+} signaling and gene expression. Ca^{2+} oscillations mediate signaling in a wide variety of cell types

Original received March 5, 2004; revision received May 11, 2004; accepted May 13, 2004.

From the Laboratories of Cardiovascular Sciences (D.B.Z., M.J., S.J.S.) and Clinical Investigation (E.K.), Gerontology Research Center, Intramural Research Program, National Institute on Aging, National Institutes of Health, Baltimore, Md; and the Department of Bioenergetics (D.B.Z.), A.N. Belozersky Institute of Physico-Chemical Biology, Moscow, Russia.

Correspondence to Steven J. Sollott, MD, or to Magdalena Juhaszova, PhD, Laboratory of Cardiovascular Science, Gerontology Research Center, Box 13, Intramural Research Program, National Institute on Aging, 5600 Nathan Shock Dr., Baltimore, MD 21224-6825. E-mail sollotts@grc.nia.nih.gov

© 2004 American Heart Association, Inc.

Circulation Research **is available at http://www.circresaha.org** **DOI: 10.1161/01.RES.0000137875.42385.8e**

Downloaded from circres.ahajournals.org by on May 24, 2010

and, unless they are synchronized (such as in the beating heart), their occurrence or nature (eg, frequency, amplitude, etc) might not be apparent from ensemble measurements. Significant information about these processes would obviously need to use a single cells studies.

Currently, one of the most useful techniques to assess the activities of individual cells, subcellular trafficking of signals to and between organelles, and to appreciate how organelle function is regulated is based on fluorescence microscopy imaging. Each of the various imaging techniques requires that the signaling molecule(s), compartment(s), or organelle(s) be labeled in a specific fashion such that they can be tracked in time and space without significantly interfering with the underlying processes. In other experiments, the combination of specialized imaging techniques together with cellular probes capable of producing photodynamic changes in the local environment enables "interactivity," because it is intentionally devised to enable dynamic perturbation of the system and to follow the responses in real time. These labels can be exogenously introduced or fortuitously may already exist as endogenous species with innate fluorescence properties that can be exploited for the purpose.

Fluorescent Probes of Cell Signaling: Small Organic Fluorophores

Aside from the fluorescent antibody techniques having few practical applications for intracellular imaging in living cells,[1] the most significant advances came from the development of small organic fluorescent molecules by Roger Tsien's laboratory that were responsive to ionic signals, such as Ca^{2+}, H^+, and membrane potential ($\Delta\Psi_m$), and could be introduced into live cells, generally without significant toxicity.[2] Many of these fluorochromes are both useful for and limited to measurements in compartments to which they would naturally distribute. Perhaps one of the most useful applications of this technology is the ability to image microdomain Ca^{2+} dynamics.[3,4] Small organic probes that have been particularly useful to assess Ca^{2+} flux include the ratiometric indicators, indo-1 and fura-2, which shift their excitation or emission spectra on binding Ca^{2+}, and the nonratiometric ("single wavelength") indicators, fluo-3 and rhod-2 (and their newer derivatives), which increase fluorescence emission on Ca^{2+} binding.[5]

Although certain indicators would naturally sequester inside-specific organelles because of biophysical or biochemical properties favoring that distribution (such as $\Delta\Psi_m$ providing the accumulation of positively charged dyes, ie, tetramethylrhodamine methyl ester [TMRM] and tetramethylrhodamine ethyl ester [TMRE], and the Ca^{2+}-indicator, rhod-2, inside mitochondria[6]), specific targeting for most of these dyes inside specific subcellular locations is generally not possible. Available fluorophores are multivalent organic anions that by themselves are impermeant to membranes. Because of this limitation, acetate-ester or acetoxymethyl-ester derivatives have been developed for these compounds, rendering them membrane-permeable and easily loaded into cells. Endogenous esterases regenerate the original organic anion form of the indicator, trapping it inside the cell.[7] Although the distribution of dye-loading can be manipulated to favor relative localization in certain compartments by controlling the temperature and hence activity of esterases during dye-loading (for example, facilitation of the relative mitochondrial localization of the marker molecule, calcein),[8] nevertheless, the highly specific localization of these ester-derivative–loaded dyes to a given compartment or organelle is frequently impractical.

Fluorescent Protein Tags and Biosensors

An important advance during the 1990s enabled the introduction of genes encoding fluorescent proteins that could serve to tag expressed proteins,[9] which proved to be well-suited for fluorescence microscopy and enabled in vivo tracking of proteins.[10] The cloning[11] and expression[9] of the jellyfish green fluorescent protein (GFP) was the first of this group and has been used extensively for real-time imaging in live cells.[12,13] In the intervening decade, GFP has undergone significant improvements; currently, a wide variety of GFP mutants are available that emit increased fluorescence, have favorably shifted spectral properties that emit light of different colors, and have improved photostability. Also, a range of fluorescent proteins from other organisms has been cloned and the application of the expression of the anemone red fluorescent protein, DsRed, has been demonstrated.[14] Recently, a "fluorescent timer" protein was identified from the mutation of a red fluorescent protein (E5), which changes from green to red over time, and thus can be used to report the timing and regulation of gene expression.[15] Mutations in a nonfluorescent chromoprotein from *Anemonia sulcata* has produced a "kindling" fluorescent protein that becomes fluorescent under moderate green light excitation. Light of greater intensity or longer duration causes irreversible kindling. With an organelle-targeted sequence (and irreversibly kindled), it may be used to report solitary organelle traffic within a cell.[16]

Another photoprotein from the jellyfish is aequorin (AEQ), which undergoes a Ca^{2+}-induced conformational change leading to the oxidation of its coenzyme, coelenterazine, and the emission of blue light (chemiluminescence).[5,17] Although AEQ has yielded valuable insights into Ca^{2+} signaling, several limitations have become apparent. Coelenterazine is consumed and the photoprotein is destroyed on Ca^{2+} binding to AEQ. Also, the inherent signal produced on Ca^{2+} binding is very low (<1 photon per molecule), creating problems with detection and limiting the spatial and temporal resolution.[18] Fluorescent protein tags and biosensors are presented in detail in another part of this thematic series.[19] However, several additional developments deserve special mention because of their importance for the present review.

Organelle-Targeted AEQs and GFPs

Organelle-targeted AEQs and GFPs can be genetically expressed in target cells; chimeric AEQs with organelle-specific targeting sequences enable cellular expression of recombinant protein to specific intracellular locations, including the cytosol,[20] nucleus,[20,21] sarcoplasmic reticulum,[22] endoplasmic reticulum,[23] mitochondria,[24,25] golgi apparatus,[26] secretory granules,[27] and gap junctions.[28] Cells can also be transfected with specific organelle-targeted GFPs,[29] and combinations of the different color GFP mutants can be used together to target

Downloaded from circres.ahajournals.org by on May 24, 2010

different organelles in the same cell.[30,31] Probes are now available for compartments, including the cytosol, endoplasmic reticulum (ER), mitochondria, golgi, nucleus, and plasma membrane.[10,32]

GFP Emission Variants

Perhaps the most important engineered GFPs manifesting different spectral properties is the production of 2 mutants, a blue-shifted cyan fluorescent protein (ECFP) and a red-shifted yellow fluorescent protein (EYFP), because they have overlapping spectra that allows fluorescence resonance energy transfer (FRET).[31,33] FRET is a quantum mechanical event describing the nonradiative energy transfer from an excited donor chromophore to an acceptor chromophore, which in turn emits light at its own wavelength.[34] This only occurs when the 2 dipoles are within a range of <10 nm. Because FRET is proportional to the sixth power of the distance between dipoles, small changes in separation of the GFP pair can induce substantial changes in the signal, making this a very sensitive reporter of the biochemical event. A potential drawback of this approach is that the probe is molecularly bulky and can interfere with the underlying phenomenon or with its targeting.

GFP-Based Ion and Second Messenger Probes

An entire range of GFP-based indicators sensitive to specific ions and second messengers has been developed.[35] These include sensors of Ca^{2+}, H^+, cAMP, cGMP, and protein kinase activity (PKA, PKC, tyrosine kinase), and those targetable to subcellular compartments and organelles. Recently, reduction—oxidation-sensitive GFPs (roGFPs) have been created with cysteines in appropriate positions to form disulfide bonds. These roGFPs have been targeted to both the cytosol and the mitochondria and display rapid and reversible ratiometric changes in fluorescence in response to changes in ambient redox potential in vitro and in vivo.[36] For the purposes of the present review, we limit the discussion to GFP-based Ca^{2+} sensors (designed around variations of GFP–calmodulin constructs): "cameleons," "camgaroos," and "pericams."[33,37–39] In each case, the sensor relies on the change in conformation on Ca^{2+}–calmodulin-binding to serve as the molecular switch. In the case of chameleon, this leads to changes in FRET between cyan fluorescent protein and yellow fluorescent protein (YFP); for the non-FRET–based camgaroo and pericam probes (each of which have only YFP [or a variant] interacting with calmodulin) Ca^{2+}-binding leads to a specific change (increase) in fluorescence of YFP. Compared with cameleons, pericams show greater Ca^{2+} responses and improved signal-to-noise ratio.[38] By contrast to low Ca^{2+}-affinity camgaroos (Kd=7 μmol/L),[37] pericams have higher Ca^{2+} affinity (Kd=0.7 μmol/L), favorable for sensing physiological Ca^{2+}changes.[38] It should also be noted that GFP-based probes are generally quite pH-sensitive, which can complicate their use. Cameleon probes have been targeted to the nucleus,[33] endoplasmic reticulum,[33] mitochondrial matrix,[40] and the plasma membrane.[41] Pericam probes have targeted to the nucleus,[39] mitochondria,[25,38] and plasma membrane.[42]

Photobleaching Methods

Photobleaching is photochemical alteration of a fluorophore resulting in depletion of fluorescence. Usually, photobleaching is performed by scanning a focused laser across defined regions of interest at high zoom and intensity. Advanced methods use an acousto-optical tunable filter, which enables rapid control of laser attenuation during scanning. Accurate measurements in defined regions of interest are achieved by rapid switching between the bleaching and normal beam.

There are different photobleaching techniques.[43] Fluorescence recovery after photobleaching (FRAP) is based on selective photobleaching of fluorophores in defined regions of interest and subsequent monitoring of recovery that occurs as nonbleached molecules move into the bleached region. It provides information about kinetics of protein diffusion, binding, and trafficking. To monitor the rate of the movement out of the bleached region, inverse FRAP is performed. Fluorophores outside the region of interest are photobleached, and fluorescence loss in nonphotobleached areas is monitored. Fluorescence localization after photobleaching (FLAP) is used with proteins tagged with 2 different fluorophores. By photobleaching 1 of these fluorophores, the movement of nonphotobleached pools can be monitored over time. In fluorescence loss in photobleaching (FLIP) experiments, defined regions of interest are repeatedly photobleached, whereas the whole cell is imaged. Cell regions interconnected with the photobleached area lose fluorescence because of movement of mobile proteins into this area, but unconnected regions are not affected.

Mitochondria

In addition to the long-recognized roles in energy metabolism, mitochondria play crucial roles in apoptosis, redox, and Ca^{2+} homeostasis. They oxidize substrates (forming a proton motive force with both $\Delta\Psi_m$ and ΔpH components), which also provide a major source of reactive oxygen species (ROS) production. $\Delta\Psi_m$ drives ATP synthesis, cation transport, and protein transport, and also is a signal in the cell life–death decision. In addition to ROS, mitochondria are a source of reactive nitrogen species (RNS) and a target regulated by nitric oxide (NO).[44,45]

Membrane Potential

All fluorescent molecules used as probes for the transmembrane potential in general (and $\Delta\Psi_m$ specifically) must meet important criteria. They should carry a delocalized charge, thus making them membrane-permeable, and should be accumulated according to the Nernst electrochemical potential:

$$\Delta\Psi_m = -\left(\frac{RT}{nF}\right)\log\left(\frac{F_{in}}{(F_{out}}\right)$$

where F_{in} and F_{out} are the concentrations of the (monovalent) cation inside and outside the organelle. These are hydrophobic or amphiphilic organic molecules, in which charge-delocalization is caused substantially by the electron density spreading across several coupled double bonds. If the compartment is charged negatively inside (eg, cell interior, mitochondrial matrix), lipophilic cations are used. Having a

Downloaded from circres.ahajournals.org by on May 24, 2010

negative membrane potential of ≈200 to 250 mV (the polarization of inner mitochondrial membrane with respect to the outside of the cell) results in mitochondria accumulating dye to levels ≈4 orders above that outside the cell (1 μmol/L outside yields >1 mmol/L in the matrix, which may be toxic[46]). Because physical diffusion through lipid barriers is required to achieve gradient levels determined by $\Delta\Psi_m$, these probes fall into the group of "slow" dyes,[47] meaning that fluorescence changes cannot immediately follow changes in $\Delta\Psi_m$. Because these permeant cations are extruded by P-glycoprotein (ie, multidrug-resistance transporter),[48] specific precautions should be taken to avoid artifacts. Another complicating property of these dyes (which actually facilitates photodynamic therapy) is "non-Nernstian" retention inside mitochondria of some tissues, making it difficult to assign an energy dependence of their accumulation.[49]

One of the oldest mitochondrial fluorochromes described is Janus green (introduced >50 years ago), although it is rarely used today because of significant toxicity. Currently, the most useful mitochondrial dyes include: those from rhodamine and rosamine families (TMRM, TMRE, rhodamine 123, tetramethylrosamine); those retained in mitochondria after chemical fixation by conjugation with proteins and lipids (mitotrackers: green, red, orange); mitoFluors (green, red) and nonylacridine orange (staining mitochondria in live and fixed cells, but unable to be retained after fixation); carbocyanines [indo- (DiI), thia- (DiS) and oxa- (DiO) derivatives]; dual-emission dyes (JC-1, JC-9) expressing their fluorescence in a potential-sensitive mode by having green fluorescent monomers under low $\Delta\Psi_m$ and red fluorescent aggregates when $\Delta\Psi_m$ is high; styryl dyes (DASPMI and DASPEI) having large fluorescence Stokes shifts; and others.

In general, many of these dyes can measure $\Delta\Psi_m$ in the steady state if used at the low submicromolar range. It should be emphasized that sufficient time for dye equilibration must be allowed. Beyond the issue of toxicity, problems arise when dyes are used at concentrations above the point at which fluorescence becomes nonlinear as a function of concentration. In fact, at micromolar bathing concentrations, rhodamines can accumulate to levels inside mitochondria at which fluorescence self-quenching is obtained, caused by increased dissipation of excitation energy by the high probability of molecular collisions, as well as the formation of dye aggregates with altered fluorescence properties. Under these circumstances, mitochondrial depolarization (causing the redistribution of dye into the cytoplasm) can produce a superficially "paradoxical" *increase* of fluorescence as the intramitochondrial dye levels decrease to levels at which self-quenching is less. Although there are useful $\Delta\Psi_m$ measurements that can be made using this "dequenching" approach, it is our opinion that the lowest dye concentration possible probably provides the general all-around best balance of experimental compromises. Additionally, each of these compounds can act as photosensitizing agents. Photodynamic effects, principally resulting from the photochemical ROS production as a byproduct of dye excitation in the presence of oxygen, can cause significant and unwanted phototoxicity without proper attention to the experimental conditions. We feel that the most useful small molecule probes for dynamic measurements of $\Delta\Psi_m$ are TMRE and TMRM used at very low concentrations. Detailed examinations of practical methods for validation and calibration of fluorescence measurements of $\Delta\Psi_m$ are available.[46,50]

Photodynamic Depolarization, Induction of the MPT, and ROS

The photodynamic effects described in the context of toxicity can also be exploited to experimental advantage to perturb cellular systems in controlled ways, for example, to examine cellular responses in real-time by the controlled local production of free radicals in specific organelles to simulate a signaling event or pathological stress. Because probes such as TMRM localize inside mitochondria and produce ROS when photoexcited, we exploited this coincidence to track $\Delta\Psi_m$ during experimentally controlled ROS-induction of the MPT, using laser line-scanning confocal microscopy imaging.[51] Repetitive laser scanning of a row of mitochondria in a cell loaded with TMRM causes additive incremental exposure of just that laser-targeted area to the photodynamic production of ROS. After a reproducible ROS exposure, the MPT occurs, which is clearly identified by the immediate dissipation of $\Delta\Psi_m$ (Figure 1A). In cardiac myocytes double-loaded with TMRM and the ROS-tracking dye, dichlorofluorescein (DCF), MPT-induction (triggered by the *photodynamic* production of ROS) coincided with a burst of *mitochondrial* ROS generation (as measured by DCF fluorescence), which we have termed mitochondrial "ROS-induced ROS release" (RIRR) (Figure 1B). Using this methodology, we examined cardioprotection signaling mechanisms. Protection involves activation of endogenous signaling, which can confer significant resistance to oxidant and other stresses associated with ischemia/reperfusion injury. We demonstrated that hypoxia/reoxygenation significantly reduces the MPT ROS threshold, that cardiac myocyte survival is steeply negatively correlated with the fraction of depolarized mitochondria, and that a wide variety of cardioprotective agents acting via distinct upstream mechanisms all promote cell survival by limiting MPT induction. We found that protection can be triggered in 2 general ways—dependent and independent of regulatory mitochondrial swelling—which converge via inhibition of GSK-3β on the end effector, the permeability transition pore complex, preventing the MPT.[52]

Because the MPT causes nonselective permeability of the inner mitochondrial membrane to solutes with molecular masses up to ≈1.5 kDa, its occurrence can be followed by the redistribution of marker molecules that are normally membrane-impermeable. The fluorescent molecule, calcein, has been found suitable for this purpose, and has enabled imaging of the MPT in situ. Calcein can be loaded into cells as the membrane-permeable acetoxymethyl ester forms, where it can enter essentially all organelles, and cellular esterases hydrolyze the dye to form the impermeable salt form. The success of the live cell-imaging method, however, relies on the ability to selectively load and entrap calcein initially with a sufficient gradient across the inner mitochondrial membrane to observe any quantitative redistribution later on MPT induction,[7,53] or be able to selectively quench the fluorescence in the cytosol (eg, with Co^{2+}) leaving the mitochondrial matrix-entrapped species fluores-

Downloaded from circres.ahajournals.org by on May 24, 2010

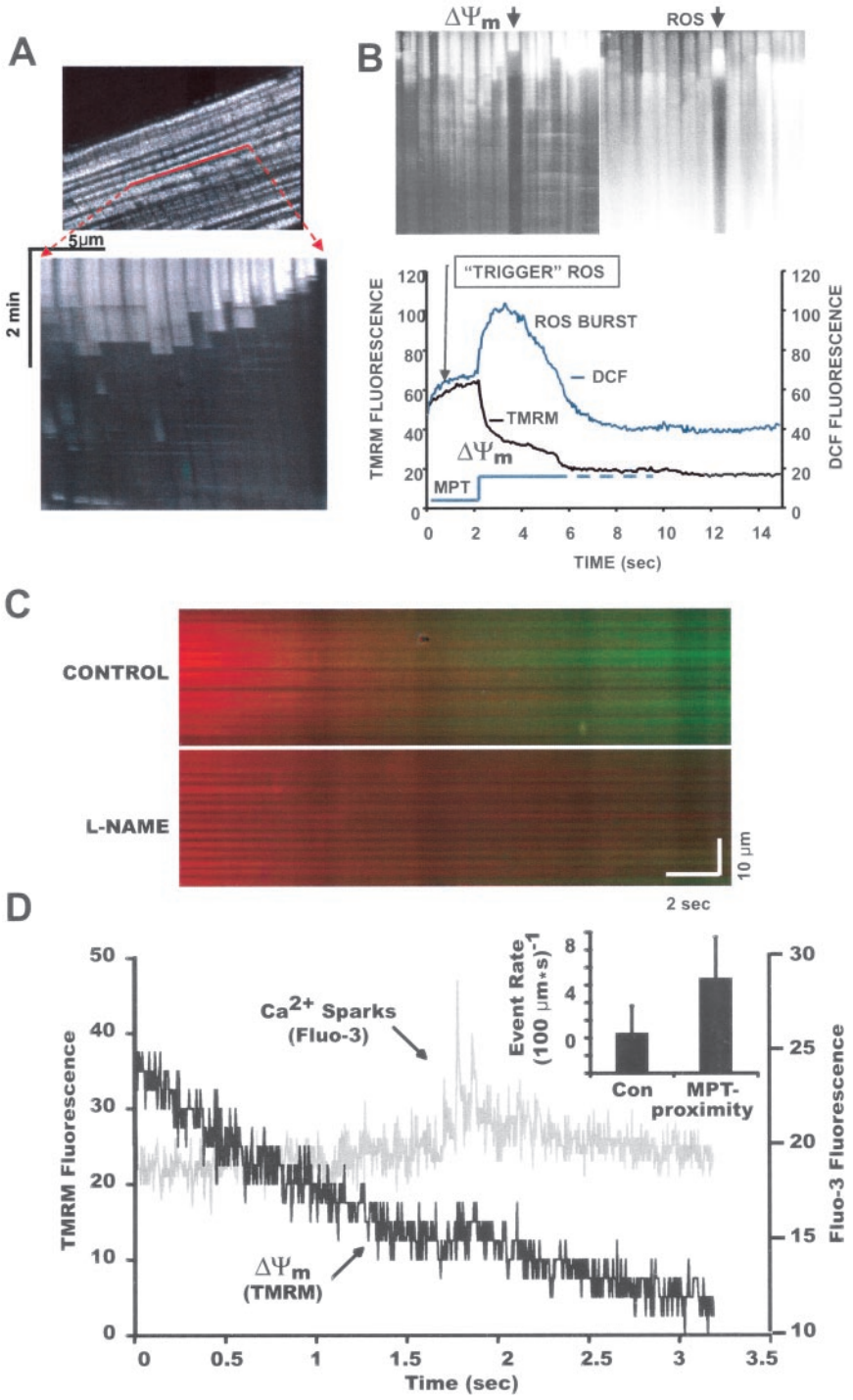

Figure 1. Linescan imaging of mitochondrial arrays, MPT-induction and ROS-induced ROS release (RIRR). A, upper panel, Confocal image of fluorescence in TMRM-loaded (125 nmol/L) cardiac myocyte. Line drawn on image shows position scanned for experiment in bottom panel. Bottom panel shows 2-Hz linescan image of TMRM fluorescence along mitochondrial row; time progresses from top. The sudden dissipation of TMRM fluorescence (white-to-black transitions) indicates mitochondrial $\Delta\Psi_m$ loss and MPT-induction. B, Linescan in myocyte dual-loaded with TMRM and DCF showing photoexcitation–ROS triggers the ROS burst after MPT induction (RIRR). C, Endogenous (mitochondrial) production of NO after MPT induction and inhibition by L-NAME. Myocytes were loaded with 125 nmol/L TMRM (red) and 10 μmol/L DAF-2 (green) and line-scanned at 100 Hz. D, Induction of Ca^{2+} sparks after the MPT. Myocyte is dual-loaded with 125 nmol/L TMRM and fluo-3 and line-scan imaged at 230 Hz. Inset, Comparison of Ca^{2+} spark rate in proximity of MPT occurrence (ie, within the sarcomere containing the involved mitochondria and within 3 seconds after MPT occurrence, vs that at background) ($P<0.05$). Reproduced from Zorov et al,[51] with permission from the *Rockefeller University Press*.

cent.[54] Although each of these techniques has some significant limitations,[53] careful application has permitted convincing MPT demonstration in direct cell imaging (Figure 2A).

Aon et al examined the propagation and consequences of RIRR in cardiac myocytes loaded with TMRE and DCF using 2-photon confocal microscopy.[55] They demonstrated that photo-induced mitochondrial depolarization and ROS-release in <1% of the volume of the cell can trigger self-propagated spatio-temporally synchronized, cyclosporin A–insensitive oscillations in $\Delta\Psi_m$, mitochondrial ROS-production, and mitochondrial redox potential (as reflected in NAD(P)H autofluorescence, see later) throughout the entire volume of the cell, which had become apparently independent of exogenous photodynamic ROS. Furthermore, these mitochondrial transitions were found to be tightly coupled to activation of sarcolemmal K_{ATP} currents, causing oscillations in action potential duration, and thus might contribute to arrhythmias during ischemia–reperfusion injury.

Imaging of Mitochondrial NO

A novel fluorometric probe, 4,5-diaminofluorescein diacetate (DAF-2DA), has been developed that enables detection of

Downloaded from circres.ahajournals.org by on May 24, 2010

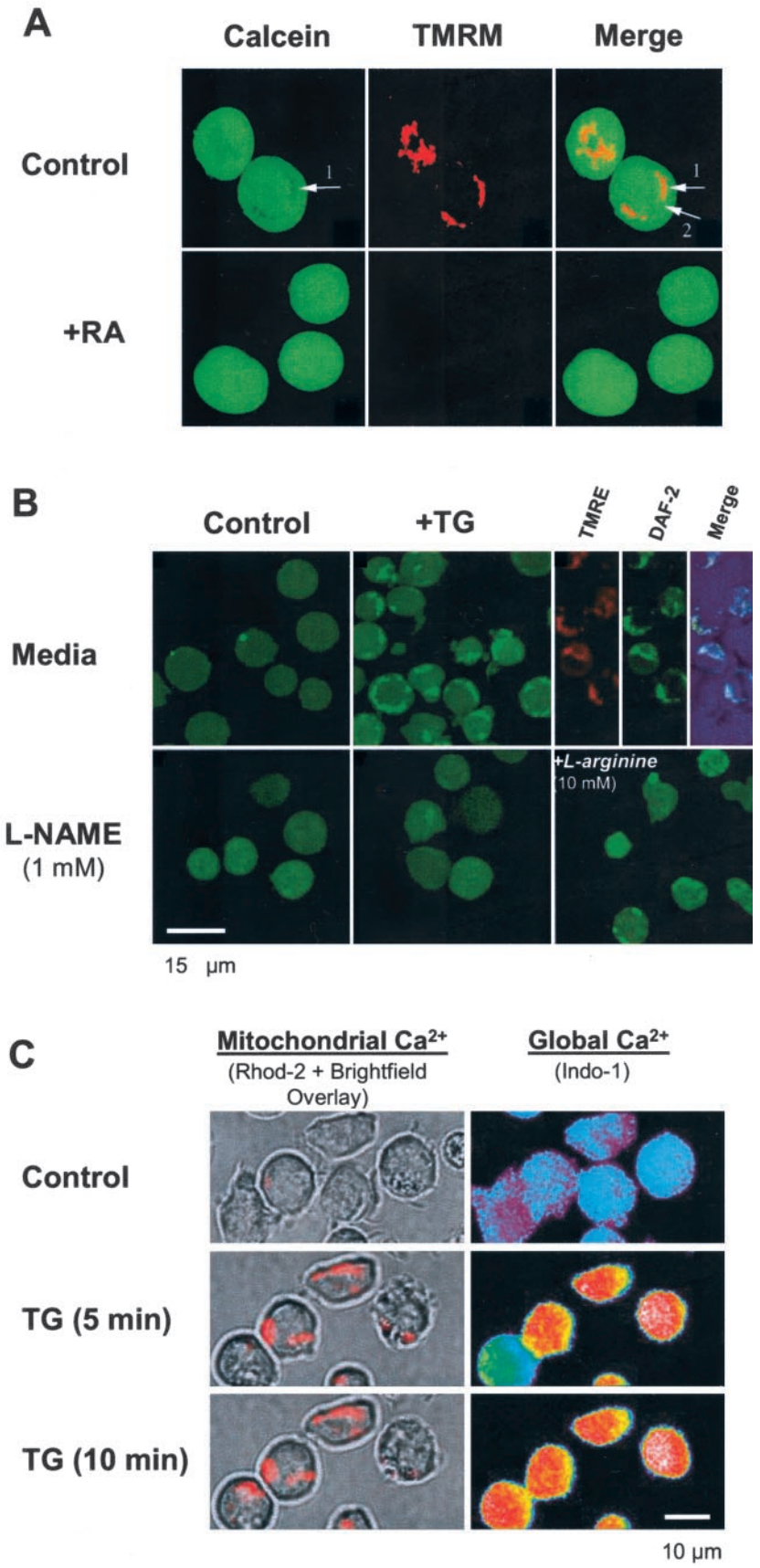

Figure 2. A, Confocal microscopy images showing Jurkat cells pinocytically loaded with calcein (green) and TMRM (red). Retinoic acid (RA) was used to induce MPT. Control cells show mitochondria remain intact with calcein unable to enter (arrows show voids in calcein where TMRM remains inside polarized mitochondria), whereas calcein gains entry to mitochondria on MPT after RA.[53] B, Mitochondria NO production in Jurkat cells loaded with DAF-2 (green) and stained with TMRE (red). Thapsigargin (50 nmol/L) induces mitochondrial NO production (colocalization of DAF-2 and TMRE), prevented by L-NAME and restored by excess L-arginine. C, Parallel increases in mitochondria and global Ca^{2+} by 50 nmol/L TG in Jurkat cells loaded with indo-1 (pseudocolor) and rhod-2 (red, with brightfield image overlay). B and C, From M.J., D.B.Z., and S.J.S., unpublished data (B: 1998; C: 1999).

Downloaded from circres.ahajournals.org by on May 24, 2010

NO production in living cells.[56] DAF-2DA is cleaved to DAF-2, trapping it within the cell. Reaction of DAF-2 with NO to form the stable triazolofluorescein DAF-2T yields a >180-fold increase in fluorescence. In experiments from our laboratory, we found that MPT-induction produces a burst of mitochondrial ROS and also a significant increase in NO production.[51] In cardiac myocytes dual-loaded with TMRM and DAF-2, a significant increase of mitochondrial DAF-2 fluorescence was observed after MPT induction, suggesting that NO production had occurred in these areas (but with relatively slower kinetics compared with the ROS burst); the specificity for NO detection in these experiments was demonstrated by ability of the NOS inhibitor, L-NAME, to abolish the increase in DAF-2 fluorescence after MPT-induction (Figure 1C).

Because oxidative and nitrosative stress can modulate the spontaneous activity of the ryanodine receptor,[57,58] we examined the nature of Ca^{2+} spark activity in the "wake" of MPT induction.[51] As shown in Figure 1D, in a representative cell dual-loaded with TMRM and the Ca^{2+}-sensitive dye, fluo-3, there is frequently a period of significantly increased Ca^{2+} spark frequency at the z-lines (ie, the site of the T-tubule–sarcoplasmic reticulum junction) in the immediate vicinity of the mitochondrion soon after MPT induction. In proximity of the MPT (defined as within the sarcomere containing the involved mitochondria and within 3 seconds after MPT occurrence), the event rate approximately doubled (Figure 1D, inset). Although ordinary background Ca^{2+} sparks are typically single events, the MPT-associated ones frequently occurred as clusters, as seen in Figure 1D. Although it is possible that mitochondrial Ca^{2+} may contribute to Ca^{2+} spark formation,[59] we were unable to exclude the possibility that such local Ca^{2+} release from sarcoplasmic reticulum (SR) may be driven by ROS/RNS generated in and released by these adjacent mitochondria undergoing MPT induction (a "ROS/RNS-induced Ca^{2+} release" mechanism). Regardless of whether Ca^{2+} or ROS modulate this increased spark frequency after MPT induction, this phenomenon could induce pathological disturbances in cardiac excitation and rhythm, for example, contributing to postischemic reperfusion arrhythmias.

Recently, it was noted that ER–Ca^{2+} stress could induce apoptosis in nonexcitable cells, such as Jurkat T-cells, in a Ca^{2+}-dependent and NO-dependent fashion.[60] Using DAF-2–loaded Jurkat cells exposed to the SERCA inhibitor, thapsigargin (TG 50 nmol/L, which results in apoptosis in approximately one-third of the population by 36 hours), together with confocal imaging, we found that mitochondria rapidly produce NO (colocalization of DAF-2 signal with TMRE added at the end of the experiment confirms mitochondrial localization; see Figure 2B) compared with control cells not TG-exposed (not shown). Specificity of NO production was provided by parallel experiments in the presence of L-NAME, which prevented the TG-related increase in mitochondrial DAF-2 fluorescence, which was restored in the presence of >10-fold L-arginine (Figure 2B).

Imaging Mitochondrial Ca^{2+} and pH

The nature of the Ca^{2+} dependence of ER–stress-mediated (TG-mediated) apoptosis was examined in Jurkat cells dual-loaded with indo-1 and rhod-2 to assess whole-cell and mitochondrial Ca^{2+}, respectively, using confocal imaging. Figure 2C shows that TG produced a rapid, parallel increase in both whole-cell and mitochondrial Ca^{2+}. We found that although Ca^{2+}-dependent activation of NO production mediates apoptosis after ER stress, and that protection against apoptosis seen in Bcl-2 and Bcl-X_L overexpressing cells was mediated not by any difference in TG-induced elevations in mitochondrial and global cell Ca^{2+}, but rather by the downstream capacity to produce NO.[60] Hajnóczky's laboratory examined the transmission of cytosolic Ca^{2+} oscillations mediated by $InsP_3$ into the mitochondrial matrix and found a tight, synapse-like functional coupling architecture, which would explain how periodic $InsP_3$ receptor activation could dynamically control Ca^{2+}-dependent mitochondrial metabolism.[61] Cytosolic Ca^{2+} signal communication to mitochondria using confocal imaging of compartmentalized rhod-2 in H9c2 cells was further examined.[62] They found that cytosolic Ca^{2+} sparks mediated by ryanodine receptors could elicit miniature mitochondrial matrix Ca^{2+} signals that they called "Ca^{2+}-marks," which are restricted to single mitochondria. A key finding was that mitochondria also appear to have a direct effect on the properties of Ca^{2+} sparks, because inhibition of mitochondrial Ca^{2+} uptake results in an increase in the frequency and duration of Ca^{2+} sparks, suggesting that mitochondrial Ca^{2+} handling may be an important determinant of cardiac excitability through local feedback control of elementary Ca^{2+} signals.

The mitochondria-targeted chimeric AEQ and GFPs have been useful for understanding mitochondrial Ca^{2+} dynamics. In an early report using mitochondrial AEQ, together with parallel fura-2 measurements to follow cytoplasmic Ca^{2+}, Rizzuto et al were able to observe that physiological stimulation with Ca^{2+}-mobilizing agents induced increases of the Ca^{2+} level in mitochondria much larger than those reached in the bulk cytoplasm.[24] Ratiometric chameleons having appropriate localization signals permitted measurement of free Ca^{2+} concentrations simultaneously in the nucleus and mitochondria, revealing that extramitochondrial Ca^{2+} transients caused rapid changes in mitochondrial Ca^{2+} together with the free propagation of Ca^{2+} across the nuclear envelope.[33] In another elegant demonstration, using mitochondrial-targeted and nuclear-targeted ratiometric pericams, Pozzan's group showed that in neonatal cardiac myocytes, mitochondrial Ca^{2+} oscillates synchronously with cytosolic Ca^{2+} and that mitochondrial Ca^{2+} handling rapidly adapts to inotropic and chronotropic inputs[25] (Figure 3).

Because the electrochemical potential energy formed by oxidative phosphorylation is stored in the H^+ gradient ($\Delta\mu_H$, which in turn is harnessed for ATP production), and hence comprises both $\Delta\Psi_m$ and ΔpH, it is important to be able to measure both variables because perturbations can influence them independently. Whereas $\Delta\Psi_m$-tracking probes are well-developed (see previous), methods to accurately measure mitochondrial matrix pH (and hence ΔpH) remain problematic. Specifically, fluorescein and its derivatives, carboxy-SNARF and BCECF, are difficult to selectively localize inside mitochondria, and although certain pH-sensitive GFPs can be appropriately targeted, many have pK_a that make them

Downloaded from circres.ahajournals.org by on May 24, 2010

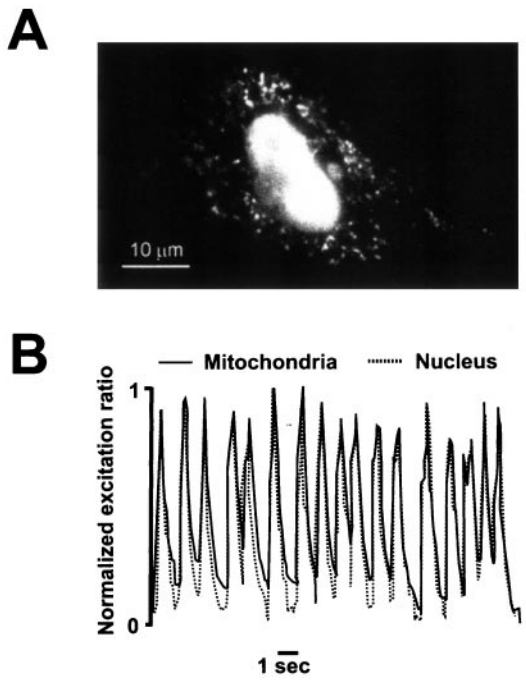

Figure 3. Spontaneous Ca^{2+} oscillations in spontaneously beating neonatal cardiac myocytes measured with "ratiometric pericams" targeted to the nucleus and the mitochondria. Reproduced from Robert et al,[25] with permission from *Nature* (http://www.nature.com/nature).

less sensitive to pH changes in the alkaline environment of the mitochondrial matrix.[63] However, a GFP chimera targeted to the mitochondria was recently engineered that has an apparent $pK_a \approx 8.5$, which develops large reversible fluorescence changes, making it suitable for use as a mitochondrial alkaline pH indicator (named "mtAlpHi").[64]

Imaging Mitochondrial Redox State

The main source of reducing equivalents to the respiratory chain is reduced nicotinamide-adenine dinucleotide (NADH). A family of flavoproteins (which deliver reducing equivalents via flavins, FAD, or FMN) is in close redox equilibrium with the mitochondrial NAD system. The NAD redox state reflects the metabolic *balance* of the rate of oxidative phosphorylation by respiration and the rate of delivery of reducing equivalents to the respiratory chain. Fortuitously, NADH is fluorescent, whereas the oxidized form, NAD^+, is not. In contrast, flavoprotein fluorescence increases with oxidation. Because of this, ratiometric fluorometry may be rather useful because 2 signals respond oppositely to changes in mitochondrial metabolic states. This kind of redox fluorimetry has been used for studying regulation and defects in cellular energy metabolism.[65] One important application of this was from Marbán's laboratory, which established single-cell methodologies to assay surface K_{ATP} and mitochondrial K_{ATP} channel activities by measuring membrane current and flavoprotein fluorescence simultaneously.[66,67] They showed that activation of the mitochondrial K_{ATP} increases flavoprotein oxidation, and that this endogenous fluorescence could be used as a reporter of mitochondrial K_{ATP} activity (Figure 4A and 4B).

Another redox fluorimetry application to characterize energy metabolism in single cardiomyocytes uses a perturbation–kinetics approach via rapid photobleaching of NADH, followed by "enzyme-dependent" FRAP confocal imaging as the topological measure of its resynthesis (Figure 4C and 4D).[68] The mono-exponential NADH recovery curve provides a pseudo first-order reaction rate constant of regional NADH generation capacity, reflecting NADH dehydrogenase activity and NADH use (in the respiratory chain and in catabolic processes), providing information beyond conventional steady-state methods.

Imaging Mitochondrial Caspase-3 Activation

Among various apoptotic components, caspases-2, 3, 8, and 9 were recently found inside mitochondria.[69,70] Uncertainty remains regarding whether "upstream" caspases and "executioner" caspase-processing takes place inside mitochondria or if they are released from mitochondria in immature form. Paradoxically, digested products of procaspase-9 have not been detected in mitochondria, whereas caspase-3 (classically "downstream" of caspase-9) was found in activated form both in cytosol and in mitochondria.[71] Furthermore, there is no information about the possibility that caspases might be activated locally to serve purposes other than apoptosis (which would be below immunoblot detection limits). Cell imaging together with different permeant fluorescent caspase substrates would be useful to address these questions. Using a permeable fluorogenic caspase substrate containing the caspase-3 recognition motif, DEVD (PhiPhiLux-G_1D_2[72]), together with TMRM loading, we observed increased DEVDase activity in areas corresponding to rare, spontaneously depolarized mitochondria in cardiomyocytes (Figure 5).

The concept of programmed *mitochondrial* destruction was put forth as a possible function of the mitochondrial megachannel (permeability transition pore)[73] and later named "mitoptosis."[74] Mitochondrial proteins have a half-life of days (depending on tissue, the slowest turnover is 17.5 days in heart and 24.4 days in brain),[75] but the process of mitochondrial execution has not been characterized (except for limited EM data identifying mitochondrial degradation in lysosomes). It is unclear whether mitochondria are executed by an "apoptosis-like" program, but we speculate that the orderly disposal of mitochondria in postmitotic cells (such as in heart and brain) requires specially compartmentalized mechanisms (possibly involving caspase-3) unless *premature* apoptosis is accidentally triggered.

Sarcoplasmic/Endoplasmic Reticulum

Previously, extensive data related to the estimation of stored SR/ER Ca^{2+} were based on indirect measurements of the released SR/ER Ca^{2+} into cytosol after activation. Development of Ca^{2+} indicator Fluo-5N (with low $K_d \approx 400$ μmol/L) facilitated direct measurements of SR Ca^{2+}, including observing the beat-to-beat dynamics of stored SR Ca^{2+} in cardiac myocytes.[76] Fluo-5N fluorescence was localized to z-lines and transverse tubules (confirmed by Di-8-ANNEPS staining).

Combination of multiple fluorescence indicators and a method to stretch cardiac myocytes (Figure 6A and 6B)

Downloaded from circres.ahajournals.org by on May 24, 2010

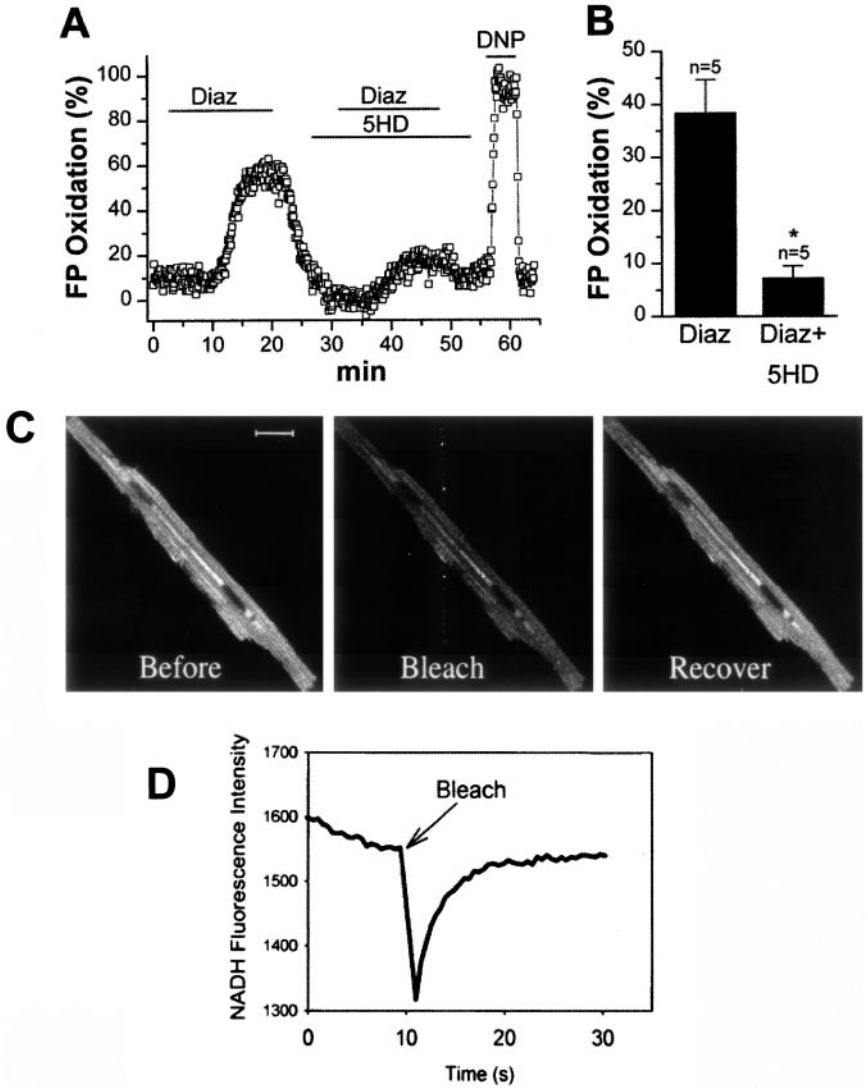

Figure 4. Mitochondrial redox-state imaging in cardiac myocytes. A and B, Effects of the mitoK$_{ATP}$ agonist, diazoxide (Diaz), and its inhibitor, 5-hydroxydecanoate (5HD), on flavoprotein (FP) fluorescence as an index of FP oxidation. Data calibrated by exposing cells to DNP. FRAP of NADH in isolated cardiac myocyte. C, NADH fluorescence intensity recovery after a bleach pulse demonstrate an apparent exponential mode (D) almost reaching a prebleaching level. A and B are reproduced from Hu et al,[67] with permission from the *American Society for Pharmacology and Experimental Therapeutics*. C and D are reproduced from Combs and Balaban,[68] with permission from the *Biophysical Society*.

permitted study of the mechanisms of stretch-dependent modulation of Ca^{2+}-transient amplitude, Ca^{2+} spark frequency, and NO production.[58] Stretch increased the amplitude of the electrically stimulated Ca^{2+} transients assessed in cells loaded with the ratiometric indicator, indo-1 (Figure 6D and 6E). To understand the mechanisms of the stretch effect on Ca^{2+} transients, spontaneous Ca^{2+} spark frequency was compared in slack and stretched myocytes loaded with indicator Fluo-3 (Figure 6C). Spontaneous Ca^{2+} spark frequency (but not amplitude) increased directly with stretch and

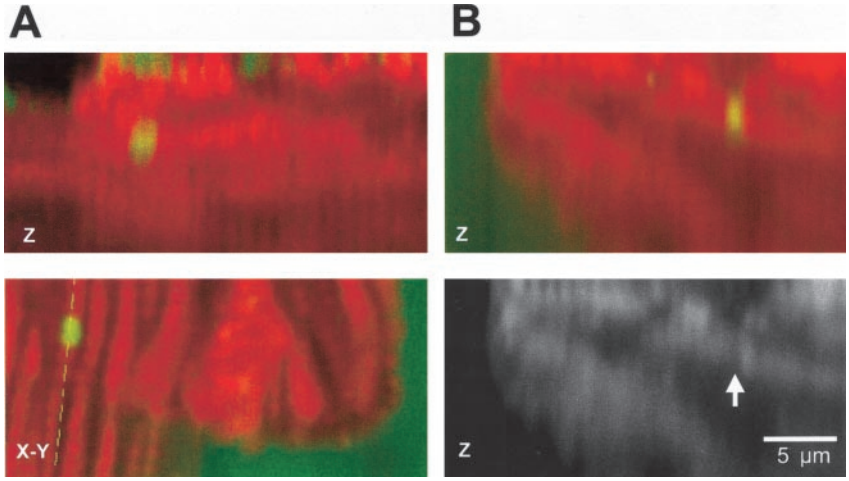

Figure 5. Imaging of the localized caspase activity in intact cardiac myocytes. A and B, Cells incubated with TMRM (red) and the permeable fluorogenic caspase substrate containing the caspase-3 recognition motif DEVD (PhiPhiLux-G$_1$D$_2$; green) showed increased DEVDase activity in areas corresponding to rare, spontaneously depolarized mitochondria (arrow in B shows TMRM channel alone). Confocal *x*–*y* vs *z* sections, as indicated on the image. From D.B.Z., M.J., and S.J.S, unpublished data, 1999.

Downloaded from circres.ahajournals.org by on May 24, 2010

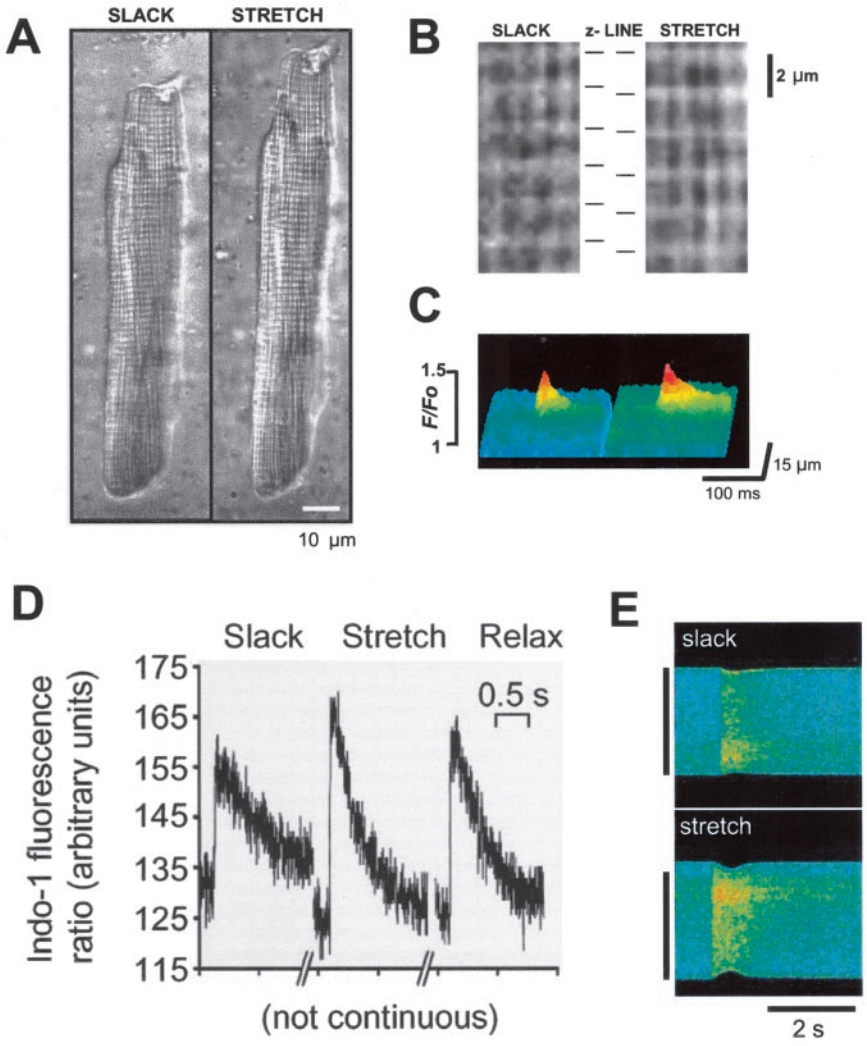

Figure 6. Stretch modulation of Ca^{2+} release properties in cardiac myocytes. A through C, Measurement of Ca^{2+} sparks in slack (left panels) and stretched (by 10%, right panels) myocytes. Enlargement of whole-cell images (A) demonstrates proportionate sarcomere-length changes with cell-stretch (B) without significant changes in signal-averaged Ca^{2+} spark characteristics (C). D and E, Indo1-loaded myocyte showing sequence of electrically stimulated Ca^{2+} transients (0.5 Hz steady-state) at slack length, 10 minutes after 9% stretch, and 10 minutes after relaxation to slack length, as measured using confocal linescan imaging (E). Cell-stretch produces a reversible increase in the Ca^{2+}-transient amplitude (D). Reproduced from Petroff et al,[58] with permission from *Nature* (http://www.nature.com/nature).

was blocked by NOS and PI(3)K inhibitors. To show that stretch directly modulated endogenous NO production, cells were loaded with DAF-2DA. Imaging experiments demonstrated that stretch induced NO production in cardiac myocytes. It was proposed that myocyte NO produced by stretch activation of the PI(3)K-Akt-eNOS axis acts as a second messenger of stretch by enhancing ryanodine receptor activity, contributing to myocardial contractile activation.[58]

In live and fixed cells, the structure and dynamics of basic elements of SR/ER (the membranous sacs, tubules, polygonal reticulum, and junctions) can be revealed with a variety of lipophilic probes. Originally, Terasaki et al used the fat-soluble dicarbocyanine dye, 3,3′-dihexyloxacarbocyanine iodide [DiOC6(3)], to study SR/ER morphology.[77] At low concentrations, DiOC6(3) accumulates preferentially into mitochondria. High concentrations are toxic for mitochondria, which condense and depolarize, releasing DiOC6(3), which then redistributes and reveals SR/ER structure. The fixable ER-Tracker Blue-White DPX indicator is a relatively selective and photostable stain for the SR/ER in live cells. Unlike DiOC6(3), ER-Tracker does not incorporate into mitochondria, and at low concentrations appears to be nontoxic.[78] Cell-permeable BODIPY FL-X- and BODIPY TR-X-conjugates of thapsigargin, ryanodine, and $InsP_3$ proved useful to study the spatial distribution and density of SR/ER ryanodine receptors,[79–81] $InsP_3$ receptors,[82] and Ca^{2+}-ATPases.[79,81,82] FRAP experiments revealed remarkable changes in the mobility of proteins in the ER lumen under conditions of cell stress,[83] thus proving ER to be a very dynamic structure responding to cell stress.

Nucleus

Transcriptional Factors

Regulation of transcription is a critical point in nuclear gene expression. There are important transcription factors that are translocated from cytoplasm to nucleus on activation. Fluorescent tags such as GFP allow time-lapse imaging of activation of transcription factor in live cells. Nuclear factor of activated T cells (NFAT) plays a central role in the development of cardiovascular system. Activation of NFAT requires nuclear Ca^{2+} elevation. Calcineurin (CaN) binds and translocates NFAT into the nucleus as a complex.[84] The distribution of NFAT between nuclear and cytoplasmic compartments is dynamically regulated by CaN and nuclear kinase activities. The stimulation-dependent nuclear translocation of GFP–NFAT has been demonstrated in skeletal

Downloaded from circres.ahajournals.org by on May 24, 2010

muscle fibers,[85] in Jurkat and BHK cells,[86] and in arterial smooth muscle.[87] Another transcription factor, NF-κB, translocates into the nucleus after phosphorylation and degradation of an inhibitory subunit, I-kB.[88] Dynamics of this translocation has been studied with a GFP–NF-κB fusion protein.[89] GFP–NF-κB also can be used in a DNA-binding assay in vitro by applying the principle of FRET.[90]

FRET-based assays can be used to detect transcriptional activation inside nucleus in situ. cAMP stimulates the expression of numerous genes through the PKA-mediated phosphorylation of the cAMP-responsive element-binding protein, CREB, which recruits the coactivator CREB binding protein (CBP).[91] To monitor the formation of the active transcriptional CREB/CBP complex, fusion constructs of CREB/CBP interacting domains (KID and KIX) with ECFP and EYFP were created, and interaction of KID and KIX domains was monitored by FRET.[92] The important role of voltage-gated L-type Ca^{2+} channels in activating of CREB-dependent transcription has been shown in neurons and in recombinant systems.[93,94]

Nuclear Organization, RNA, and Protein Transport

Different photobleaching techniques revealed a highly dynamic nuclear organization. FRAP and FLIP experiments showed that several nuclear proteins involved in ribosomal biogenesis cycle rapidly between the nucleolus and nucleoplasm.[95] These findings of the dynamic nature of nuclear structure particularly highlight the need for the application of advanced imaging techniques with sufficient spatial and temporal resolution.

Many aspects of posttranscriptional regulation of gene expression involve specific RNA–protein interactions. Selective RNA recognition by GFP sequence-specific RNA binding protein fusion constructs serves as a reliable indicator of RNA localization.[96] With this technique, it is possible to visualize RNAs that are synthesized and processed by cells.[97] Nuclear pore permeability of 27-kDa EGFP was examined by real-time FRAP imaging. In this elegant study, no evidence for significant nuclear pore gating or block of EGFP diffusion by depletion of perinuclear Ca^{2+} stores was found, as assayed by a perinuclear-targeted Ca^{2+} indicator.[98]

Nuclear Calcium

Interplay between cytoplasmic and nuclear Ca^{2+} regulation remains controversial. Ryanodine and $InsP_3$ receptors are reported[99] to participate in Ca^{2+} release from the nuclear envelope. Nucleus-targeted cDNAs encoding fluorescent protein calcium indicators (cameleons) were transfected into suprachiasmatic nucleus neurons. Circadian rhythm changes were observed for the cytosolic Ca^{2+} reporter, but not for the nuclear one,[100] indicating that the nucleoplasmic reticulum regulates calcium signals independently of cytosol. Two-photon uncaging of $InsP_3$ revealed spatially restricted PKC signaling for the nucleus and cytoplasm. PKC was translocated from cytoplasm to the plasma membrane by photorelease of Ca^{2+} into the cytoplasm. Photorelease of Ca^{2+} into the nucleus induced a loss of nucleoplasmic PKC, which relocated to the nuclear envelope. These findings showed that the nuclear interior contains a network of calcium stores forming functionally distinct subcomparments.[101] See the online data supplement, available at http://circres.ahajournals.org, for fluorescence applications in "Other Organelles."

Recent Advances

Nanoscopy

A weakness of fluorescence microscopy lies in its relatively low spatial resolution, which is limited by light diffraction to approximately one-half of the wavelength of excitation or emission light (the Rayleigh criterion). Going beyond this limit requires advanced technical measures, which theoretically can resolve 2 points in the fluorescent image separated by a distance less than the diffraction limit. There are 3 approaches to obtain this resolution enhancement: (1) specialized optical devices; (2) image processing; and (3) special fluorescent probes or physico-chemical processes for generation of the recorded signal,[102,103] for example, Quantum dots (see later). Using these approaches, resolution to ≈28 nm can theoretically be achieved (see the online data supplement).

Quantum Dots

Existing imaging techniques use small organic fluorescent molecules, fluorescent biomolecules, and photoproteins. However, their spectral properties limit the use of >3 dyes at a time to tag and image different biological molecules simultaneously. Fluorescence of dyes also tends to fade away quickly over time. Inorganic semiconductor nanocrystals, "quantum dots" (QDs) (2 to 10 nm, on the order of average proteins), have intriguing optical properties that get around these problems and have the potential to revolutionize biological imaging. In addition to being brighter and persisting longer than organic fluorophores, QDs have a broader excitation spectrum. This means that a mixture of different QDs can be excited by a single-wavelength light source, allowing simultaneous detection and imaging in color. When the electron-hole pairs in the core of a QD are excited with a beam of light, they emit fluorescence that depends directly on the size of the dot: the larger the dot, the redder the light. Thus, QDs can be fine-tuned to emit light at a variety of wavelengths (compatible with standard fluorescent microscopes) simply by altering the core size.

Stable, soluble, and biocompatible cadmium–selenide QDs encapsulated in phospholipid micelles were developed and tested for the first time in Xenopus embryos.[104] On cell division, QDs appeared to be solely distributed to the offspring of the injected parent cell and did not appear to have any detrimental effect on the frog development. The dots were stable for months in vivo, fluorescence could be followed to the tadpole stage, allowing cell-lineage tracking experiments throughout embryogenesis without significant photobleaching.

Recently Quantum Dot Corporation developed QD conjugates with streptavidin, protein A, biotin, IgGs, small molecules, and oligonucleotides. These bioconjugates are well-suited for multicolor applications because of to their narrow (typically 20 to 40 nm) and symmetric emission spectra and are a promising alternative to organic dyes for fluorescence-based applications (Figure 7). QDs linked to streptavidin and

Downloaded from circres.ahajournals.org by on May 24, 2010

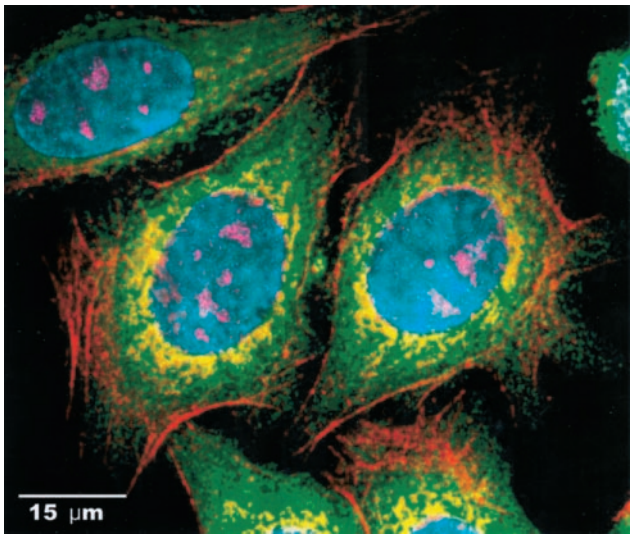

Figure 7. Simultaneous 5-color imaging in fixed human epithelial cells using QD conjugates. The colors allowed localization of cellular proteins and substructures: nuclei (cyan), cell proliferation protein Ki-67 (magenta), mitochondria (orange), microtubules (green), and actin filaments (red). Courtesy of Quantum Dot Corp. (Hayward, Calif).

IgG were successfully used to label the breast cancer marker Her2 on the surface of fixed and live cancer cells, to stain actin and microtubule fibers in the cytoplasm, and to detect nuclear antigens inside the nucleus.[105]

QD labeling has enabled real-time assessment of protein trafficking in living cells. QDs have been used to track the motional dynamics of individual glycine receptors in neurons.[106] Much larger probes would not have worked, as the receptors are only ≈5 nanometers wide. The ability to image QD-tagged glycine receptors by real-time fluorescence and by electron microscopy allowed both dynamic behavior and accurate localization studies to be performed with the same samples. Epidermal growth factor-conjugated QDs enabled tracking the dynamics of the interaction and activation of the EGF receptor, erbB1, in real time.[107] Two-photon microscopy of QDs was used by Larson et al[108] to image capillary blood flow through the skin of live mice.

These examples illustrate that the properties of QDs make them suitable for applications in many areas from tagging single proteins in cells to diagnostic imaging, with great potential for use in diverse fluorescence applications and in emerging imaging technologies.

Conclusion

Previously, anatomical and physiological studies defined the ability of organs and certain aspects of cellular function in vivo to change in time in response to perturbations, but considerable molecular mechanistic detail was lacking. Twentieth and twenty-first century advances in molecular biology and genetics identified many key molecules involved in signal transduction, and often linear and sometimes branching, network hierarchies can be deduced, but what is ultimately desired, the coordinated integration in cells in space and time, is frequently beyond the reach of these techniques alone. This review has attempted to show by example how the synergy of these disciplines and advanced microscopy imaging has provided one of the most useful techniques to assess the activities of individual cells, subcellular trafficking of signals to and between organelles, and to appreciate how organelle function is regulated. The future of "molecular imaging" appears bright, with such novel interdisciplinary applications as QDs from solid-state physics, super-resolution optics enabling nanoscale resolution, and developments from other disciplines, providing new opportunities in signal tracking from cells to animals. From "Animalcules" to QDs, Léeuwenhoek would be proud.

Acknowledgments

This work was supported by the Intramural Research Program, National Institute on Aging, National Institutes of Health.

References

1. Farinas J, Verkman A. Receptor-mediated targeting of fluorescent probes in living cells. *J Biol Chem*. 1999;274:7603–7606.
2. Tsien RY. Fluorescent probes of cell signaling. *Annu Rev Neurosci*. 1989;12:227–253.
3. Bers DM Dynamic imaging in living cells: windows into local signaling. *Sci STKE*. 2003;177:PE13.
4. Dolmetsch R. Excitation-transcription coupling: signaling by ion channels to the nucleus. *Sci STKE*. 2003;166:PE4.
5. Takahashi A, Camacho P, Lechleiter JD, Herman B. Measurement of intracellular calcium. *Physiol Rev*. 1999;79:1089–1125.
6. Minta A, Kao JP, Tsien RY. Fluorescent indicators for cytosolic calcium based on rhodamine and fluorescein chromophores. *J Biol Chem*. 1989; 264:8171–8178.
7. Lemasters JJ, Trollinger DR, Qian T, Cascio WE, Ohata H. Confocal imaging of Ca^{2+}, pH, electrical potential, and membrane permeability in single living cells. *Methods Enzymol*. 1999;302:341–358.
8. Ohata H, Chacon E, Tesfai SA, Harper IS, Herman B, Lemasters JJ. Mitochondrial Ca^{2+} transients in cardiac myocytes during the excitation-contraction cycle: effects of pacing and hormonal stimulation. *J Bioenerg Biomembr*. 1998;30:207–222.
9. Chalfie M, Tu Y, Euskirchen G, Ward WW, Prasher DC. Green fluorescent protein as a marker for gene expression. *Science*. 1994;263: 802–805.
10. Tsien RY. The green fluorescent protein. *Annu Rev Biochem*. 1998;67: 509–544.
11. Prasher DC, Eckenrode VK. Ward W W, Prendergast FG Cormier MJ. Primary structure of the Aequorea victoria green-fluorescent protein. *Gene*. 1992;111:229–233.
12. Rizzuto R, Brini M, Pizzo P, Murgia M, Pozzan T. Chimeric green fluorescent protein as a tool for vizualizing subcellular organelles in living cells. *Curr Biol*. 1995;5:635–642.
13. Lippincott–Schwartz J, Snapp E, Kenworthy A. Studying protein dynamics in living cells. *Nature Rev Mol Cell Biol*. 2001;2:444–456.
14. Matz MV, Fradkov AF, Labas YA, Savitsky AP, Zarajsky AG, Markelov ML, Lukyanov SA. Fluorescent proteins from nonbioluminescent Anthozoa species. *Nature Biotechnol*. 1999;17:969–973.
15. Terskikh A, Fradkov A, Ermakova G, Zaraisky A, Tan P, Kajava AV, Zhao X, Lukyanov S, Matz M, Kim S, Weissman I, Siebert P. "Fluorescent timer": protein that changes color with time. *Science*. 2001;290: 1585–1588.
16. Chudakov DM, Belousov VV, Zaraisky AG, Novoselov VV, Staroverov DB, Zorov DB, Lukyanov S, Lukyanov KA. Kindling fluorescent proteins for precise in vivo photolabeling. *Nat Biotechnol*. 2003;21: 191–194.
17. Woods NM, Cuthbertson KS, Cobbold PH. Repetitive transient rises in cytoplasmic free calcium in hormone stimulated hepatocytes. *Nature*. 1986;319:600–602.
18. Shimomura O, Johnson FH. Calcium binding, quantum yield, and emitting molecule in aequorin bioluminescence. *Nature*. 1970;227: 1356–1357.
19. Zaccolo M. Use of chimeric fluorescent proteins and fluorescence resonance energy transfer to monitor cellular responses. *Circ Res*. 2004; 94:866–873.

Downloaded from circres.ahajournals.org by on May 24, 2010

20. Badminton MN, Campbell AK, Rembold CM. Differential regulation of nuclear and cytosolic Ca^{2+} in HeLa cells. *J Biol Chem*. 1996;271: 31210–31214.
21. Brini M, Murgia M, Pasti L, Piscard D, Pozzan T, Rizzuto R. Nuclear Ca^{2+} concentration measured with specifically targeted recombinant aequorin. *EMBO J*. 1993;12:4813–4819.
22. Robert V, De Giorgi F, Massiimino ML, Cantini M, Pozzan T. Direct monitoring of the calcium concentration in the sarcoplasmic and endoplasmic reticulum of skeletal muscle myotubes. *J Biol Chem*. 1998;273: 30372–30378.
23. Montero M, Brini M, Marsault R, Alvarez J, Sitia R, Pozzan T, Rizzuto, R. Monitoring dynamic changes in free Ca^{2+} concentration in the endoplasmic reticulum of intact cells. *EMBO J*. 1995;14:5467–5475.
24. Rizzuto R, Simpson AW, Brini M, Pozzan T. Rapid changes of mitochondrial Ca^{2+} revealed by specifically targeted recombinant aequorin. *Nature*. 1992;358:325–327.
25. Robert V, Gurlini P, Tosello V, Nagai T, Miyawaki A, Di Lisa F, Pozzan T. Beat-to-beat oscillations of mitochondrial [Ca^{2+}] in cardiac cells. *EMBO J*. 2001;20:4998–5007.
26. Pinton P, Pozzan T, Rizzuto R. The Golgi apparatus is an inositol 1,4,5-trisphosphate-sensitive Ca^{2+} store, with functional properties distinct from those of the endoplasmic reticulum. *EMBO J*. 1998;17: 5298–5308.
27. Pouli AE, Karagenc N, Wasmeier C, Hutton JC, Bright N, Arden S, Schofield JG, Rutter GA. A phogrin-aequorin chimera to image free Ca^{2+} in the vicinity of secretory granules. *Biochem J*. 1998;330: 1399–1404.
28. George CH, Kendall JM, Campbell AK Evans WH. Connexin-aequorin chimerae report cytoplasmic calcium environments along trafficking pathways leading to gap junction biogenesis in living COS-7 cells. *J Biol Chem*. 1998;273:29822–29829.
29. De Giorgi F, Ahmed Z, Bastianutto C, Brini M, Jouaville LS, Marsault R, Murgia M, Pinton P, Pozzan T, Rizzuto R. Targeting GFP to organelles. *Methods Cell Biol*. 1999;58:75–85.
30. Rizzuto R, Brini M, De Giorgi F, Rossi R, Heim R, Tsien RY, Pozzan T. Double labelling of subcellular structures with organelle-targeted GFP mutants in vivo. *Curr Biol*. 1996;6:183–188.
31. Zhang J, Campbell RE, Ting AY, Tsien RY. Creating new fluorescent probes for cell biology. *Nature Rev Mol Cell Biol*. 2002;3:906–918.
32. Chalfie M, Kain S. Green fluorescent protein. Properties, applications, and protocols. New York: Wiley-Liss & Sons, Inc; 1998.
33. Miyawaki A, Llopis J, Heim R, McCaffery JM, Adams JA, Ikura M, Tsien RY. Fluorescent indicators for Ca^{2+} based on green fluorescent proteins and calmodulin. *Nature*. 1997;388:882–887.
34. Forster T. Energiewandering and Fluoreszenz. *Naturwissenschaffer*. 1946;33:166–175.
35. Pozzan T, Mongillo M, Rudolf R. The Theodore Bucher lecture. Investigating signal transduction with genetically encoded fluorescent probes. *Eur J Biochem*. 2003;270:2343–2352.
36. Hanson GT, Aggeler R, Oglesbe D, Canon M, Capaldi RA, Tsien RY, Remington SJ. Investigating mitochondrial redox potential with redox-sensitive green fluorescent protein indicators. *J Biol Chem*. 2004;279: 13044–13053.
37. Baird GS, Zacharias DA, Tsien RY. Circular permutation and receptor insertion within green fluorescent proteins. *Proc Natl Acad Sci U S A*. 1999;96:11241–11246.
38. Nagai T, Sawano A, Park ES, Miyawaki A. Circularly permuted green fluorescent proteins engineered to sense Ca^{2+}. *Proc Natl Acad Sci U S A*. 2001;98:3197–3202.
39. Nakai J, Ohkura M, Imoto K. A high signal-to-noise Ca^{2+} probe composed of a single green fluorescent protein. *Nat Biotechnol*. 2001; 19:137–141.
40. Arnaudeau S, Kelley WL, Walsh JV Jr., Demaurex N. Mitochondria recycle Ca^{2+} to the endoplasmic reticulum and prevent the depletion of neighboring endoplasmic reticulum regions. *J Biol Chem*. 2001;276: 29430–29439.
41. Emmanouilidou E, Teschemacher AG, Pouli AE, Nicholls LI, Seward EP, Rutter GA. Imaging Ca^{2+} concentration changes at the secretory vesicle surface with a recombinant targeted cameleon. *Curr Biol*. 1999; 9:915–918.
42. Pinton P, Tsuboi T, Ainscow EK, Pozzan T, Rizzuto R, Rutter, GA. Dynamics of glucose-induced membrane recruitment of protein kinase C beta II in living pancreatic islet beta-cells. *J Biol Chem*. 2002;277: 37702–37710.
43. Lippincott-Schwartz J, Altan-Bonnet N, Patterson GH. Photobleaching and photoactivation: following protein dynamics in living cells. *Nat Cell Biol*. 2003;Suppl:S7–S14.
44. Ghafourifar P, Richter C. Nitric oxide synthase activity in mitochondria. *FEBS Lett*. 1997;418:291–296.
45. Boveris A, Costa LE, Poderoso JJ, Carreras MC, Cadenas E. Regulation of mitochondrial respiration by oxygen and nitric oxide. *Ann NY Acad Sci*. 2000;899:121–135.
46. Scaduto RC Jr., Grotyohann LW. Measurement of mitochondrial membrane potential using fluorescent rhodamine derivatives. *Biophys J*. 1999;76:469–477.
47. Waggoner AS. Dye indicators of membrane potential *Annu Rev Biophys Bioeng*. 1979;8:47–68.
48. Diddens H, Gekeler V, Neumann M, Niethammer D. Characterization of actinomycin-D-resistant CHO cell lines exhibiting a multidrug-resistance phenotype and amplified DNA sequences. *Int J Cancer*. 1987;40:635–642.
49. Summerhayes IC, Lampidis TJ, Bernal SD, Nadakavukaren JJ, Nadakavukaren KK, Shepherd EL, Chen LB. Unusual retention of rhodamine 123 by mitochondria in muscle and carcinoma cells. *Proc Natl Acad Sci U S A*. 1982;79:5292–5296.
50. O'Reilly CM, Fogarty KE, Drummond RM, Tuft RA, Walsh JV Jr. Quantitative analysis of spontaneous mitochondrial depolarizations. *Biophys J*. 2003;85:3350–3357.
51. Zorov DB, Filburn CR, Klotz LO, Zweier JL, Sollott SJ. Reactive oxygen species (ROS)-induced ROS release: a new phenomenon accompanying induction of the mitochondrial permeability transition in cardiac myocytes. *J Exp Med*. 2000;192:1001–1014.
52. Juhaszova M, Zorov DB, Kim S-H, Pepe S, Fu Q, Fishbein KW, Ziman BD, Wang S, Ytrehus K, Antos CL, Olson EN, Sollott SJ. GSK-3β mediates convergence of protection signaling to inhibit the mitochondrial permeability transition pore. *J Clin Invest*. 2004;113: 1535–1549.
53. Jones RA, Smail A, Wilson MR. Detecting mitochondrial permeability transition by confocal imaging of intact cells pinocytically loaded with calcein. *Eur J Biochem*. 2002;269:3990–3997.
54. Petronilli V, Miotto G, Canton M, Brini M, Colonna R, Bernardi P, Di Lisa F. Transient and long-lasting openings of the mitochondrial permeability transition pore can be monitored directly in intact cells by changes in mitochondrial calcein fluorescence. *Biophys J*. 1999;76: 725–734.
55. Aon MA, Cortassa S, Marban E, O'Rourke B. Synchronized whole cell oscillations in mitochondrial metabolism triggered by a local release of reactive oxygen species in cardiac myocytes. *J Biol Chem*. 2003;278: 44735–44744.
56. Kojima, H, Nakatsubo N, Kikuchi K, Kawahara S, Kirino Y, Nagoshi H, Hirata Y, Nagano T. Detection and imaging of nitric oxide with novel fluorescent indicators: diaminofluoresceins. *Anal Chem*. 1998;70: 2446–2453.
57. Xu L, Eu JP, Meissner G, Stamler JS. Activation of the cardiac calcium release channel (ryanodine receptor) by poly-S-nitrosylation. *Science*. 1998;279:234–237.
58. Petroff MG, Kim SH, Pepe S, Dessy C, Marban E, Balligand JL, Sollott SJ. Endogenous nitric oxide mechanisms mediate the stretch dependence of Ca^{2+} release in cardiomyocytes. *Nat Cell Biol*. 2001;3:867–873.
59. Bowser DN, Minamikawa T, Nagley P, Williams DA. Role of mitochondria in calcium regulation of spontaneously contracting cardiac muscle cells. *Biophys J*. 1998;75:2004–2014.
60. Srivastava RK, Sollott SJ, Khan L, Hansford R, Lakatta EG, Longo DL. Bcl-2 and Bcl-X(L) block thapsigargin-induced nitric oxide generation, c-Jun NH(2)-terminal kinase activity, and apoptosis. *Mol Cell Biol*. 1999;19:5659–5674.
61. Csordas G, Thomas AP, Hajnoczky G. Quasi-synaptic calcium signal transmission between endoplasmic reticulum and mitochondria. *EMBO J*. 1999;18:96–108.
62. Pacher P, Thomas AP, Hajnoczky G. Ca^{2+} marks: miniature calcium signals in single mitochondria driven by ryanodine receptors. *Proc Natl Acad Sci U S A*. 2002;99:2380–2385.
63. Takahashi A, Zhang Y, Centonze E, Herman B. Measurement of mitochondrial pH in situ. *Biotechniques*. 2001;30:804–815.
64. Cano Abad MF, Di Benedetto G, Magalhaes PJ, Filippin L, Pozzan T. Mitochondrial pH monitored by a new engineered GFP mutant. *J Biol Chem*. 2004;279:11521–11529.

Downloaded from circres.ahajournals.org by on May 24, 2010

65. Balaban R S, Mandel LJ. Optical methods for the study of metabolism in intact cells. In Noninvasive Techniques in Cell Biology. J. K. Foskett, and S. Grinstein, editors. New York: Wiley-Liss; 1990:213–236.
66. Sato T, O'Rourke B, Marban E. Modulation of mitochondrial ATP-dependent K^+ channels by protein kinase C. *Circ Res*. 1998;83: 110–114.
67. Hu H, Sato T, Seharaseyon J, Liu Y, Johns DC, O'Rourke B, Marban E. Pharmacological and histochemical distinctions between molecularly defined sarcolemmal KATP channels and native cardiac mitochondrial KATP channels. *Mol Pharmacol*. 1999;55:1000–1005.
68. Combs CA, Balaban RS. Direct imaging of dehydrogenase activity within living cells using enzyme-dependent fluorescence recovery after photobleaching (ED-FRAP). *Biophys J*. 2001;80:2018–2028.
69. Mancini M, Nicholson DW, Roy S, Thornberry NA, Peterson EP, Casciola-Rosen LA, Rosen A. The caspase-3 precursor has a cytosolic and mitochondrial distribution: implications for apoptotic signaling. *J Cell Biol*. 1998;140:485–1495.
70. Susin SA, Lorenzo HK, Zamzami N, Marzo I, Brenner C, Larochette N, Prevost MC, Alzari PM, Kroemer G. Mitochondrial release of caspase-2 and -9 during the apoptotic process. *J Exp Med*. 1999;189:381–394.
71. Chandra D, Tang DG. Mitochondrially localized active caspase-9 and caspase-3 result mostly from translocation from the cytosol and partly from caspase-mediated activation in the organelle. Lack of evidence for Apaf-1-mediated procaspase-9 activation in the mitochondria. *J Biol Chem*. 2003;278:17408–17420.
72. Komoriya A, Packard BZ, Brown MJ, Wu ML, Henkart PA. Assessment of caspase activities in intact apoptotic thymocytes using cell-permeable fluorogenic caspase substrates. *J Exp Med*. 2000;191:1819–1828.
73. Zorov DB, Kinnally KW, Tedeschi H. Voltage activation of heart inner mitochondrial membrane channels. *J Bioenerg Biomembr*. 1992;24: 119–124.
74. Skulachev VP. Mitochondrial physiology and pathology; concepts of programmed death of organelles, cells and organisms. *Mol Aspects Med*. 1999;20:139–184.
75. Menzies RA, Gold PH. The turnover of mitochondria in a variety of tissues of young adult and aged rats. *J Biol Chem*. 1971;246:2425–2429.
76. Shannon TR, Guo T, Bers DM. Ca^{2+} scraps: local depletions of free $[Ca^{2+}]$ in cardiac sarcoplasmic reticulum during contractions leave substantial Ca^{2+} reserve. *Circ Res*. 2003;93:40–45.
77. Terasaki M, Song J, Wong JR, Weiss MJ, Chen LB. Localization of endoplasmic reticulum in living and glutaraldehyde-fixed cells with fluorescent dyes. *Cell*. 1984;38:101–108.
78. Cole L, Davies D, Hyde GJ, Ashford AE. ER-Tracker dye and BODIPY-brefeldin A differentiate the endoplasmic reticulum and golgi bodies from the tubular-vacuole system in living hyphae of Pisolithus tinctorius. *J Microsc*. 2000;197:239–249.
79. Coussin F, Macrez N, Morel JL, Mironneau J. Requirement of ryanodine receptor subtypes 1 and 2 for Ca(2+)-induced Ca(2+) release in vascular myocytes. *J Biol Chem*. 2000;275:9596–9603.
80. Zhang X, Wen J, Bidasee KR, Besch HR Jr., Wojcikiewicz RJ, Lee B, Rubin RP. Ryanodine and inositol trisphosphate receptors are differentially distributed and expressed in rat parotid gland. *Biochem J*. 1999; 340:519–527.
81. Inoue M, Sakamoto Y, Fujishiro N, Imanaga I, Ozaki S, Prestwich GD, Warashina A. Homogeneous Ca^{2+} stores in rat adrenal chromaffin cells. *Cell Calcium*. 2003;33:19–26.
82. Csordas G, Hajnoczky G. Sorting of calcium signals at the junctions of endoplasmic reticulum and mitochondria. *Cell Calcium*. 2001;29: 249–262.
83. Nehls S, Snapp EL, Cole NB, Zaal KJ, Kenworthy AK, Roberts TH, Ellenber J, Presley JF, Siggia E, Lippincott-Schwartz J. Dynamics and retention of misfolded proteins in native ER membranes. *Nature Cell Biol*. 2000;2:288–295.
84. Shibasaki F, Price ER, Milan D, McKeon F. Role of kinases and the phopshatase calcineurin in the nuclear shuttling of transcription factor NF-AT4. *Nature*. 1996;382:370–373.
85. Liu Y, Cseresnyes Z, Randall WR, Schneider MF. Activity-dependent nuclear translocation and intranuclear distribution of NFATc in adult skeletal muscle fibers. *J Cell Biol*. 2001;155:27–39.
86. Tomida T, Hirose K, Takizawa A, Shibasaki F, Iino M. NFAT functions as aworking memory of Ca^{2+} signals in decoding Ca^{2+} oscillation. *EMBO J*. 2003;22:3825–3832.
87. Gomez MF, Gonzalez Bosc LV, Stevenson AS, Wilkerson MK, Hill-Eubanks DC, Nelson MT. Constitutively elevated nuclear export activity opposes Ca^{2+}-dependent NFATc3 nuclear accumulation in vascular smooth muscle. *J Biol Chem*. 2003;278:46847–46853.
88. Stancovski I, Baltimore D. NF-kappaB activation: the I kappaB kinase revealed? *Cell*,. 1997;91:299–302.
89. Schmid JA, Birbach A, Hofer-Warbinek R, Pengg M, Burner U, Furtmuller PG, Binder BR, deMartin R. Dynamics of NF kappa B and Ikappa Balpha studied with green fluorescent protein (GFP) fusion proteins. Investigation of GFP-p65 binding to DNA by fluorescence resonance energy transfer. *J Biol Chem*. 2000;275:17035–17042.
90. Birbach A, Gold P, Binder BR, Hofer E, de Martin R, Schmid JA. Signaling molecules of the NF-κB pathway shuttle constitutively between cytoplasm and nucleus. *J Biol Chem*. 2002;277:10842–10851.
91. Shaywitz AJ, Greenberg ME. CREB: A stimulus-induced transcription factor activated by a diverse array of extracellular signals. *Annu Rev Biochem*. 1999;68:821–861.
92. Mayr BM, Canettieri G, Montminy MR. Distinct effects of cAMP and mitogenic signals on CREB-binding protein recruitment impart specificity to target gene activation via CREB. *Proc Natl Acad Sci U S A*. 2001;98:10936–10941.
93. Dolmetsch RE, Pajvani U, Fife K, Spotts JM, Greenberg ME. Signaling to the nucleus by an L-type calcium channel-calmodulin complex through the MAP kinase pathway. *Science*. 2001;294:333–339.
94. Kobrinsky E, Schwartz E, Abernethy DR, Soldatov NM. Voltage-gated mobilty of the Ca^{2+} channel cytoplasmic tails and its regulatory role. *J Biol Chem*. 2003;278:5021–5028.
95. Phair RD, Mistely T. High mobility of proteins in the mammalian cell nucleus. *Nature*. 2000;404:604–609.
96. Bertrand E, Chartrand P, Schaefer M, Shenoy S, Singer R, Long R. Localization of ASH1 mRNA particles in living yeast. *Mol Cell*. 1998; 2:437–445.
97. Boulon S, Basyuk E, Blanchard J-M, Bertrand E, Verheggen C. Intranuclear RNA trafficking: insights from live cell imaging. *Biochimie*. 2002;84:805–813.
98. Wei X, Henke VG, Strubing C, Brown EB, Clapham DE. Real-time imaging of nuclear permeation by EGFP in single intact cells. *Biophys J*. 2003;84:1317–1327.
99. Gerasimenko JV, Maruyama Y, Yano K, Dolman NJ, Tepikin AV, Petersen OH, Gerasimenko OV. NAADP mobilizes Ca^{2+} from a thapsigargin-sensitive store in the nuclear envelope by activating ryanodine receptors. *J Cell Biol*. 203;163:271–282.
100. Ikeda M, SugiyamaT, Wallace CS, Gompf HS, Yoshioka T, Miyawaki A, Allen CN. Circadian dynamics of cytosolic and nuclear Ca^{2+} in single suprachiasmatic nucleus neurons. *Neuron*. 2003;38:253–263.
101. Echevarria W, Leite MF, Guerra MT, Zipfel WR, Nathanson MH. Regulation of calcium signals in the nucleus by a nucleoplasmic reticulum. *Nature Cell Biol*. 2003;5:440–446.
102. Hell SW. Toward fluorescence nanoscopy. *Nat Biotechnol*. 2003;21: 1347–1355.
103. Michalet X, Lacoste TD, Weiss S. Ultrahigh-resolution colocalization of spectrally separable point-like fluorescent probes. *Methods*. 2001;25: 87–102.
104. Dubertret B, Skourides P, Norris DJ, Noireaux V, Brivanlou AH, Libchaber A. In vivo imaging of quantum dots encapsulated in phospholipid micelles. *Science*. 29;298:1759–1762.
105. Wu X, Liu H, Liu J, Haley KN, Treadway JA, Larson JP, Ge N, Peale F, Bruchez MP. Immunofluorescent labeling of cancer marker Her2 and other cellular targets with semiconductor quantum dots. *Nat Biotechnol*. 2003;21:41–46.
106. Dahan M, Levi S, Luccardini C, Rostaing P, Riveau B, Triller A. Diffusion dynamics of glycine receptors revealed by single-quantum dot tracking. *Science*. 2003;302:442–445.
107. Lidke DS, Nagy P, Heintzmann R, Arndt-Jovin DJ, Post JN, Grecco HE, Jares-Erijman EA, Jovin TM Quantum dot ligands provide new insights into erbB/HER receptor-mediated signal transduction *Nat Biotechnol*. 2004;22:198–203.
108. Larson DR, Zipfel WR, Williams RM, Clark SW, Bruchez MP, Wise FW, Webb WW. Water-soluble quantum dots for multiphoton fluorescence imaging in vivo. *Science*. 2003;300:1434–1436.

Downloaded from circres.ahajournals.org by on May 24, 2010

Supplementary Material

Other organelles

Recent progress in understanding intra- and inter-organelle dynamics in live cells has been facilitated by the development of a variety of fluorescent methods (see main text). Photobleaching techniques provide a powerful method to study the dynamics of protein trafficking[1]. FRAP imaging has been used to show that Golgi is a highly dynamic organelle with proteins continuously exchanged with the cytoplasm every 30-60 seconds[2]. The interaction of peroxisomal proteins PEX3 and PEX19 fused to ECFP and EYFP has been visualized by FRET imaging during peroxisome biogenesis[3]. The non-specific lipid transfer protein (nsL-TP) is involved in lipid transport. After synthesis in the cytoplasm, pre-nsL-TP is imported into the peroxisomes via a receptor-mediated process and cleaved into nsL-TP. FRET between microinjected Cy3-pre-nsL-TP and Cy5 labeled antibodies against peroxisomal enzymes allowed tracking of specific associations between different enzymes in the peroxisomes[4]. Jaswal et al. [5] visualized ER, Golgi apparatus, Golgi-derived vesicles, late endosomes, early endosomes, and lysosomes by expressing fluorescently tagged reporter proteins in living cells. They employed total internal reflection fluorescence microscopy (TIR-FM) to study the behavior of these organelles near the cell surface (within 100 nm with a high signal-to-noise ratio) in response to Ca^{2+} stimulation. TIR-FM allowed detection of a peripheral population of lysosomes that showed Ca^{2+}-dependent exocytosis.

Fluorescent protein tags are used to mark various cellular compartments (see main text): GFP fused to human beta 1,4-galactosyltransferase for labeling Golgi apparatus[6,7]; to NH2-terminus of human growth hormone containing four FK506 modified binding domains for labeling post-Golgi vesicles[8]; GFP-endobrevin (endobrevins are involved in endo/exocytosis of insulin) for labeling early endosomes[9]; GFP-RAB5 for labeling early endosomes and phagosomes and GFP- Rab7 for labeling late endosomes[10]; and GFP fused to a peptide containing the membrane-targeting sequence of peroxysomal ascorbate peroxidase, for labeling peroxysomes[11].

In addition Molecular Probes has developed a variety of fluorescent markers for labeling intracellular organelles in live cells. LysoTracker and LysoSensor Probes can be used to study the dynamic aspects of lysosome biogenesis and function in live cells. LysoTracker probes, which comprise

Downloaded from circres.ahajournals.org by on May 24, 2010

a fluorophore linked to a weak base that is only partially protonated at neutral pH, are permeant to cell membranes and are highly selective for acidic organelles (and effective for labeling at nanomolar concentrations). LysoSensor probes are fluorescent pH indicators that partition into acidic organelles. In contrast to the LysoTracker probes that are not sensitive to acidic pH, LysoSensor probes exhibit a pH-dependent increase in fluorescence upon acidification. Fluorescent ceramide analogs can be used for selective staining of Golgi apparatus in live cells.

Approaches towards nanoscopy

Application of standard light microscopy imaging has inherent limitations because of the physical problem of *micro*-scale resolution (i.e., limited by the diffraction of light). Standard wide-field microscopy can achieve spatial resolutions of ~0.5 :m laterally and ~1.6 :m axially. On the other hand, confocal and two-photon microscopy can achieve spatial resolutions of ~0.25 :m laterally and ~0.7 :m axially. In addition to techniques involving advanced, specialized fluorescent probes such as quantum dots (see main text), there are two other general approaches to obtain improved resolution from light microscopy, several theoretically able to yield nanoscale resolution which will be discussed below. This section is provided to serve as an brief introduction to this topic, and the reader is encouraged to examine the reference material for further details.

1) ***Optical devices.*** In fluorescence microscopy the real focusing spot is never spherical, but can be described mathematically as a point-spread function (PSF) that results in a significant difference in an axial and lateral resolution in a ratio of about 3:1. The Fourier transform of the PSF describes the spatial frequencies transferred by the microscope. “Interference” methods give a more narrow excitation volume along the optical axis, which results in a significant improvement of the axial resolution. In “image interference” microscopy (I^2M) a fluorescent sample is placed between two opposing objective lenses, each focused on the same focal plane thus giving two magnified images that can be combined by a beam splitter and directed onto the CCD camera. “Incoherent interference illumination” microscopy (I^3M) uses spatially incoherent light sources, and excitation light illuminates the sample from both sides. The two

interference methods employed in I^2M and I^3M are independent and can be used in the same setup simultaneously (so-called "I^5M"). Modification of the optical setup through using I^5M in a wide-field, non-confocal microscope[12] (i.e., combination of I^2M with I^3M) can correct the PSF to be spherical, and in turn, achieve better resolution. Recent improvements have been obtained by using laterally structured illumination[13] (as an improved I^5M). This approach employs excitation light that varies with position. The structure of the illumination can be organized in one direction by using a stripe pattern thus giving better lateral resolution. For 2D structural illumination either rotation of the stripe pattern in many directions, or a more sophisticated pattern that covers all direction at once, are used.

Other instrumentation that has been developed to improve spatial resolution incorporates confocal microscopy with different modifications: single-photon scanning microscopy[14], theta microscopy[15], spot-scanning 4Pi[16] and two-photon microscopy[17], and a modification referred to as STED ("stimulated emission depletion" microscopy)[17]. In conventional confocal microscopy the excitation light is a maximally focused laser beam (which can be scanned across the field of interest), while the emitted light (returning through the same lens) is passed through a small, properly placed aperture (pinhole) before the detector at the objective back focal plane which rejects out-of-focus light[14]. The emission from out-of-focus planes will not go through the pinhole that enhances axial resolution compared to wide-field microscopes. The lateral resolution is also improved up to 2 fold compared to wide-field microscopy. Theta microscopy operates via the same basic principals of confocal microscopy, except that the sample is observed through an additional lens placed at right angles to the illumination lens[15]. In this case, the axial and lateral resolution is almost the same which makes the resolution of the system less anisotropic and more spherical. 4Pi-confocal fluorescence microscopy is claimed to have 3-7 times better resolution in the axial direction than the conventional confocal microscopy. It uses another concept for resolution extension, by gathering light over a different, and preferably larger, set of angles around the sample, typically by adding a second objective lens on the back side of the sample slide[16]. Merging the light collected from the specimen through both the primary and secondary lenses on the beam splitter gives two beams which can interfere; the analysis of this interference provides additional information not available in a conventional confocal microscope. The resolution is claimed to improve to an impressive 25

Downloaded from circres.ahajournals.org by on May 24, 2010

nm.

Two- (or multi-) photon absorption microscopy uses high energy excitation laser light forcing a fluorophore molecule to absorb two (or more) photons virtually simultaneously[17]. An apparent advantage is due to the fact that the infrared laser light used for multiphoton excitation undergoes less intrinsic scattering (relative to bluer wavelengths of light) which permits deeper penetration into the sample. At the same time, because the probability of the simultaneous absorption of more that one photon is insignificant in out-of-focus planes, these regions are not exposed to high intensity light capable of photochemical excitation, so the overall problem of the fluorophore photobleaching is significantly reduced. In practical terms, when compared with a single-photon confocal microscope, the resolution in a two-photon system tends to be slightly lower (when used without a pinhole before the detector).

STED provides a further ~30% improvement in lateral resolution beyond that obtained even in the enhanced confocal microscopy techniques described above. It exploits the photochemical process of "saturated quenching" of excited molecules at the periphery of a scanning focal spot, which effectively reduces the emission spot size up to 6 times beyond the diffraction limit thus practically breaking the diffraction barrier[18]. Using STED at wavelengths of 750-800 nm achieves ~28 nm lateral resolution.

2) ***Image processing techniques*** have been developed for deblurring the image (deconvolution)[19]. The goal of this approach is to reduce the out-of-focus light through a computational approach. In general, the procedure requires acquisition of images of fluorescent point-like probes having dimensions smaller than their emission wavelength to measure the optical PSF for the system. Once the PSF has been determined, 3D images of the specimen of interest are collected and processed using a deconvolution algorithm that reconstructs an idealized image based on the reassignment of photons assuming that the blurring at each point in space had occurred in accordance with a 3D distribution predicted by the PSF (there are more than 10 different deconvolution algorithms presently available, some particularly computationally demanding, incorporating different reconstruction models based on various approximations together with varying degrees of analytical rigor). These usually produce results with improved contrast and reduced background haze coming from out-of-focus fluorescence[20]. We will mention some of them. 1) Nearest-neighbor (NN) or no-neighbors deconvolution. In this approach, three

Downloaded from circres.ahajournals.org by on May 24, 2010

consecutive images are used to deconvolve the middle image. The top and bottom images are considered as windows in which out-of-focus haze from two neighboring images must pass to reach the middle image. Briefly, it is a subtraction method, in which the signal from the two adjacent planes is subtracted from the plane of interest. It is one of the easiest approaches, with the lowest cost in resources and time; 2) Linear methods such as inverse filtering, Weiner filters, and linear least squares. It is one of the simplest methods using 3D information from all focal planes to solve the imaging equations; 3) Full iterative methods utilizing PSF-based correction of all image planes of interest plus adjacent planes above and below the planes of interest; 4) "Blind" deconvolution methods using maximum-likelihood statistics, which do not assume or utilize the PSF. The resolution reached by the deconvolution methods is claimed to be around 100 nm.

Coda

These advanced approaches have been employed to gain insight into the fine structure of intracellular organelles. There are many excellent applications of such methodology presented in a number of reviews and original papers covering live specimens, imaging mitochondria and Golgi (e.g., imaging the 3D organization with much finer optical sectioning than with conventional confocal microsopy[21-23], reaching 100 nm resolution using 4Pi microscopy which proved useful to track the structural plasticity of these organelles); stained live bacteria with about 190 nm in axial resolution using 4Pi microscopy[16]; and the fine structure of cytoskeletal systems with better than 100 nm axial resolution using 3D reconstruction from images obtained via I^5M microscopy[12,13] or STED-4Pi microscopy[16,18] with the pixel size of less than 100 nm.

REFERENCES

1. Lippincott-Schwartz J. Altan-Bonnet N, Patterson GH. Photobleaching and photoactivation: following protein dynamics in living cells. *Nature Cell Biol.* 2003;Suppl.;S7-S14.

2. Ward TH, Polishchuk RS, Caplan S, Hirschberg K, Lippincott-Schwartz J. Maintenance of Golgi

Downloaded from circres.ahajournals.org by on May 24, 2010

structure and function depends on the integrity of ER export. *J Cell Biol.* 2001;155:557-570.

3. Muntau AC, Roscher AA, Kunau WH, Dodt G. The interaction between human PEX3 and PEX19 characterized by fluorescence resonance energy transfer (FRET) analysis. *Eur J Cell Biol.* 2003;82;333-342.

4. Wouters FS, Bastiaens PI, Wirtz KW, Jovin TM. FRET microscopy demonstrates molecular association of non-specific lipid transfer protein (nsL-TP) with fatty acid oxidation enzymes in peroxisomes. *EMBO J*. 1998;17;7179-7189.

5. Jaiswal JK, Andrews NW, Simon SM. Membrane proximal lysosomes are the major vesicles responsible for calcium-dependent exocytosis in nonsecretory cells.J Cell Biol. 2002, 159;625-635.

6. Llopis J, McCaffery JM, Miyawaki A, Farquhar MG, Tsien RY. Measurement of cytosolic, mitochondrial, and Golgi pH in single living cells with green fluorescent proteins. *Proc Natl Acad Sci USA.* 1998;95;6803-6808.

7. Zaal KJ, Smith CL, Polishchuk RS, Altan N, Cole NB, Ellenberg J, Hirschberg K, Presley JF, Roberts TH, Siggia E, Phair RD, Lippincott-Schwartz J. Golgi membranes are absorbed into and reemerge from ER during mitosis. *Cell.* 1999;99;589-601.

8. Rivera VM, Wang X, Wardwell S, Courage NL, Volchuk A, Keenan T, Holt DA, Gilman M, Orci L, Cerasoli F Jr, Rothman JE, Clackson T. Regulation of protein secretion through controlled aggregation in the endoplasmic reticulum. *Science*. 2000;287:826-830.

9. Nagamatsu S, Nakamichi Y, Watanabe T, Matsushima S, Yamaguchi S, Ni J, Itagaki E, Ishida H. Localization of cellubrevin-related peptide, endobrevin, in the early endosome in pancreatic beta cells and its physiological function in exo-endocytosis of secretory granules. *J Cell Sci*. 2001;114:219-227.

10. Barbero P, Bittova L, Pfeffer SR. Visualization of Rab9-mediated vesicle transport from endosomes to the trans-Golgi in living cells. *J Cell Sci*. 2002;156:511-518.

11. Lisenbee CS, Karnik SK, Trelease RN. Overexpression and mislocalization of a tail-anchored GFP redefines the identity of peroxisomal ER. *Traffic.* 2003;4:491-501.

12. Gustafsson MG, Agard DA, Sedat JW. I^5M: 3D widefield light microscopy with better than 100 nm axial resolution. *J Microsc*. 1999;195:10-16.

Downloaded from circres.ahajournals.org by on May 24, 2010

13. Gustafsson MG. Extended resolution fluorescence microscopy. *Curr Opin Struct Biol.* 1999;9:627-634.

14. Pawley JB (Ed) Handbook of biological confocal microscopy. New York: Plenum Press; 1995.

15. Lindek S, Stefany T, Stelzer EHK. Single-lens theta microscopy - a new implementation of confocal theta microscopy. *J. Microsc.* 1997; 280-284.

16. Bahlmann K, Jakobs S, Hell SW. 4Pi-confocal microscopy of live cells. *Ultramicroscopy.* 2001;87:155-164.

17. Konig K. Multiphoton microscopy in life sciences. *J Microsc*. 2000;200:83-104.

18. Dyba M, Jakobs S, Hell SW. Immunofluorescence stimulated emission depletion microscopy. *Nat Biotechnol*. 2003;21:1303-1304.

19. Carrington WA, Lynch RM, Moore ED, Isenberg G, Fogarty KE, Fay FS. Superresolution three-dimensional images of fluorescence in cells with minimal light exposure. *Science*. 1995;268:1483-1487.

20. McNally JG, Karpova T, Cooper J, Conchello JA. Three-dimensional imaging by deconvolution microscopy. *Methods*. 1999;19:373-385.

21. Hell SW. Toward fluorescence nanoscopy. *Nat Biotechnol.* 2003;21:1347-1355.

22. Egner A, Jakobs S, Hell SW. Fast 100-nm resolution three-dimensional microscope reveals structural plasticity of mitochondria in live yeast. *Proc Natl Acad Sci U S A.* 2002;99:3370-3375.

23. Egner A, Verrier S, Goroshkov A, Soling HD, Hell SW. 4Pi-microscopy of the Golgi apparatus in live mammalian cells. J.Struct.Biol. 2004;147:70-76.

Downloaded from circres.ahajournals.org by on May 24, 2010